

Contents lists available at ScienceDirect

International Journal of Mechanical Sciences

journal homepage: www.elsevier.com/locate/ijmecsci



Towards a unified approach to nonlocal elasticity via fractional-order mechanics



Sansit Patnaik*, Sai Sidhardh, Fabio Semperlotti

School of Mechanical Engineering, Ray W. Herrick Laboratories, Purdue University, West Lafayette, IN 47907, United States

ARTICLE INFO

Keywords: Fractional calculus Nonlocal elasticity Strain-gradient elasticity Stiffening Softening

ABSTRACT

This study presents a fractional-order continuum mechanics approach that allows combining selected characteristics of nonlocal elasticity, typical of classical integral and gradient formulations, under a single frame-invariant framework. The resulting generalized theory is capable of capturing both stiffening and softening effects and it is not subject to the inconsistencies often observed under selected external loads and boundary conditions. The governing equations of a 1D continuum are derived by continualization of the Lagrangian of a 1D lattice subject to long-range interactions. This approach is particularly well suited to highlight the connection between the fractional-order operators and the microscopic properties of the medium. The approach is also extended to derive, by means of variational principles, the governing equations of a 3D continuum in strong form. The positive definite potential energy, characteristic of our fractional formulation, always ensures well-posed governing equations. This aspect, combined with the differ-integral nature of fractional-order operators, guarantees both stability and the ability to capture dispersion without requiring additional inertia gradient terms. The proposed formulation is applied to the static and free vibration analyses of either Timoshenko beams or Mindlin plates. Numerical results, obtained by a fractional-order finite element method, show that the fractional-order formulation is able to model both stiffening and softening response in these slender structures. The numerical results provide the foundation to critically analyze the physical significance of the different fractional model parameters as well as their effect on the response of the structural elements.

1. Introduction

Several experimental studies have demonstrated that size-dependent effects can become prominent in the response of several structures independently of their spatial scale. In the case of micro- and nanostructures, size-dependent effects have been traced back to material heterogeneity, geometric effects such as changes in curvature, and the existence of surface and interface stresses due to nonlocal atomic interactions and Van der Waals forces [1-3]. Micro- and nano-structures such as carbon nanotubes, thin films and monolayer graphene sheets have farreaching applications in atomic devices, micro/nano-electromechanical devices, as well as sensors and biological implants. In macroscale applications, particularly those involving heterogeneous structures such as functionally graded materials, metallic foams, granular materials, and porous materials, nonlocal effects have been shown to result from material heterogeneity and interactions between different structural layers [4-7]. Additionally, specific geometric configurations can also lead to size-dependent effects [8-10]. In all these macroscopic structures, nonlocal governing equations arise following a homogenization process [5,6,9,10]. Based on the examples above, it appears that the ability to

accurately model size-dependent effects has profound implications for many engineering applications.

From a general perspective, it is the coexistence of different spatial scales in the above mentioned classes of structural problems that renders the response nonlocal [11,12]. The inability of the classical (i.e. local) continuum theory to capture scale effects prevented its use in these applications and fostered the development of the so-called nonlocal continuum theories. From a general standpoint, the mathematical description of nonlocal continuum theories relies on the introduction of additional contributions in terms of either integrals or gradients of strain (or stress) fields or to the use of additional kinematic descriptors in the constitutive equations. This approach leads to the so-called æstrongg integral methods or æweakg gradient/microcontinuum methods, respectively. Microcontinuum theories such as the Cosserat theory and the micropolar theory account for nonlocal behaviour by enriching the kinematics of the continuum with additional descriptors such as micro-rotations. Consequently, the couple-stresses, which are conjugated to the micro-rotations, are also included in the equations of motion [13–16]. Gradient elasticity theories [11,17–19] account for the nonlocal behavior by introducing strain or stress gradient dependent terms in the stress-strain constitutive law. Integral methods [12,20,21] capture

E-mail addresses: spatnai@purdue.edu (S. Patnaik), fsemperl@purdue.edu (F. Semperlotti).

^{*} Corresponding author.

nonlocal effects by re-defining the constitutive law in the form of a convolution integral of either the strain or the stress field over the horizon of nonlocality. The gradient and integral approaches are further classified as strain-driven or stress-driven [19–21], depending on whether the nonlocal contributions are modeled using the strain or the stress fields.

Although these different approaches to nonlocal elasticity have been able to address a multitude of aspects typical of the response of sizedependent nonlocal structures, some important challenges still remain open. From a high level perspective, gradient theories provide a satisfactory description of the effects of the material microstructure but can introduce significant difficulties connected with the overall stability of the model. As discussed in Askes and Aifantis [19], while the use of unstable strain-gradients is critical to capture dispersive wave propagation, they give rise to non-convex potential energies leading to the loss of uniqueness in static boundary value problems (BVPs). This issue is often circumvented by using a combination of stable strain-gradients and acceleration gradients [19,22,23], whose stability comes at the cost of additional terms in both the governing equation and the boundary conditions. From this perspective, integral methods are better suited to deal with boundary conditions and do not lead to any sign paradox, which is peculiar of the gradient methods. However, the corresponding potential energy is not guaranteed to be positive definite, and leads to illposed governing equations and inconsistent predictions for certain loading and boundary conditions [21,24,25]. The ill-posed behaviour can be addressed using local-nonlocal two phase approaches [26]. However, this effect is nullified when the local fraction vanishes, as also noted in Romano et al. [25]. More specifically, in the limit of a vanishing local fraction, the inherent ill-posedness of fully strain-driven integral problem is not eliminated. This consideration is at the basis of restrictions on the parameter space that determines the ratio of the local and nonlocal mixture.

From a perspective of practical application, another key limitation of classical nonlocal formulations consists in the fact that, based on the underlying formulation, they can capture only softening or stiffening response but not both simultaneously. Experimental investigations have shown that the size-dependent effects can lead to both stiffening as well as softening of the nonlocal structure depending on the loading and external conditions, such as temperature, loading rate, and boundary conditions [1-5,12,19,27-30]. To this regard, while classical straindriven integral formulations [20] are suitable for modeling softening effects, stress-driven integral formulations [21] and gradient formulations [11] are suitable to capture only stiffening effects. Thus it appears that both the classical integral and gradient formulations are not suitable to capture both stiffening and softening responses. Efforts to achieve an equivalence between the strain-driven integral and gradient formulations, by using special exponential kernels, have been shown to lead to mathematically ill-posed formulations resulting in inaccurate (often called "paradoxical") predictions [21,25]. Further, as stated in Askes and Aifantis [19], an unresolved issue in strain-gradient formulations pertains to the treatment of materials that exhibit strain-softening.

A recently developed nonlocal gradient elasticity approach [31] was shown to be able to capture both stiffening and softening response. In this approach, Eringen's integral law was combined with strain-gradient elasticity to formulate a higher-order nonlocal theory. More specifically, the stress is defined as the sum of two integral terms. The first term being the classical convolution between the strain and a smoothing kernel depending on a nonlocal parameter. The second term consisting of the derivative of the convolution of the strain gradient with a smoothing kernel depending on a different nonlocal parameter. The seminal work presented in Lim et al. [31] was further extended to develop strain-driven [32,33] and stress-driven approaches [34]. While the nonlocal gradient formulations capture both stiffening and softening response, some important limitations follows from the corresponding numerical implementation. Quadrature methods [33] and analytical methods [32] are the most accredited techniques for the strain-driven nonlocal gradient elasticity, while the stress-driven approach relies either on analytical solutions or iterative methods [34,35]. Although these solution methods offer analytical insights into the problem, they encounter limitations when applied to structures having more complex geometry (even plates) and general loading conditions. Further, the nonlocal strain-driven gradient approach is not positive-definite for all loading conditions and requires additional constitutive boundary conditions to achieve well-posedness when applied to slender structures of practical interest [36]. Hence, a formulation which is capable of capturing both stiffening and softening response, and amenable to numerical simulation for complex geometries under general loading conditions is still lacking.

In recent years, fractional calculus has emerged as a powerful mathematical tool to model a variety of nonlocal and multiscale phenomena. Fractional derivatives, which are a differ-integral class of operators, are intrinsically multiscale and provide a natural way to account for nonlocal effects. Given the multiscale nature of fractional operators, fractional calculus has found several applications in nonlocal elasticity [6,7,37–44]. Recent studies have shown that a nonlocal continuum approach based on fractional-order kinematic relations provides an effective way to model softening response in nonlocal structures [44,45]. These fractional-order nonlocal continuum models result in frame-invariant, thermodynamically consistent and positive definite systems with well-posed governing equations [44–46].

In this study, we show that the differ-integral nature of fractional operators allows them to combine the strengths of both gradient and integral based methods while at the same time addressing a few important shortcomings of both the integer-order formulations. More specifically, we extend the fractional-order continuum formulation [7,45] to capture both softening and stiffening response of nonlocal structures in a unified and stable formulation amenable to finite element solution. The overall goal of this study is three fold.

First, we derive the fractional-order governing equations for a 1D nonlocal continuum by continualization of the Lagrangian of a 1D lattice exhibiting long-range interactions with a power-law decay. We will show that fractional-order derivatives of the displacement field (i.e. the nonlocal strain) and fractional-order derivatives of the strain field (i.e. the strain-gradient) are obtained in the potential energy of the 1D structure following continualization of the lattice potential energy. Further, we will demonstrate that the fractional-order formulation is well-posed, frame-invariant, causal, and able to capture anomalous attenuation-dispersion characteristics without the need to resort to acceleration gradient terms, as required in classical strain-gradient formulations or the need to ensure non-vanishing strain-gradients, as required in the nonlocal strain-gradient formulation. In other terms, in the fractional-order formulation, well-posed governing equations result from a positive definite potential energy while the ability to capture dispersive behavior follows from the differ-integral nature of the fractional operator. More specifically, the attenuation and dispersion in a solid following the fractional-order formulation are shown to exhibit a power-law dependency on the wave-number/frequency. Remarkably, such anomalous dispersion characteristics have been experimentally observed in different classes of materials including lossy media, fractal and porous materials [47,48], and animal tissues [47]. Anomalous attenuation has also been observed in several (non-lossy) scattering media, particularly those characterized by fractal, periodic or random structures [7,8,10,49]. Table 1 provides a comparative summary of the classical as well as the fractional-order approaches to nonlocal elasticity, and highlights some of the most distinctive features of the methods.

A second important contribution of this study consists in extending the 1D formulation to a fully 3D formulation. The governing equations in strong form will be derived by using variational principles. In both the 1D and the 3D formulations, we will demonstrate the positive definite and convex nature of the system's potential energy. This specific property ensures that the governing equations derived by minimization of the potential energy are naturally well-posed without requiring additional constitutive boundary conditions (unlike nonlocal strain-gradient approaches). Additionally, we will discuss the frame-invariance of the

Table 1
Summary of the fundamental approaches to nonlocal elasticity and comparison of their properties with those of the fractional-order continuum theory. In the table, S.G. denotes strain gradients and I.G. denotes inertia gradients.

Features\Approach type	Integral		Gradient			
	Strain driven	Stress driven	Stable S.G.	Unstable S.G.	Stable S.G. and I.G.	Fractional
Nature of response	Soft	Stiff	Stiff	Stiff	Stiff	Soft and Stiff
Positive definite system	No	No	Yes	No	Yes	Yes
Capture dispersion	Yes	Yes	No	Yes	Yes	Yes

formulation and the complete nature of the nonlocal kernel for bounded 3D domains.

A third key contribution of this work consists in the application of the fractional-order formulation to the analysis of the static and free vibration response of Timoshenko beams and Mindlin plates. The selection of these specific formulations was due to the fact that both the Euler-Bernoulli beam and the Kirchhoff plate formulations can be recovered as special cases; hence, making our study more general and complete. By extending the fractional-order finite element method [44,45] to include the additional gradient terms, we will demonstrate that the fractional-order formulation allows modeling both stiffening and softening effects. We will also critically analyze how the overall structural behavior is affected by the different parameters introduced by the fractional model.

The characteristics discussed above also explain the choice of a strain-based fractional-order model versus a potential stress-based approach. While in integer-order techniques, the stress-based formulation [34] has been proposed as a way to address the challenging well-posedness of the nonlocal elasticity problem, the fractional order strain-based formulation is always well-posed (contrarily to its integerorder counterpart). Certainly, a stress-based fractional order formulation could potentially be envisioned. However, the corresponding methodologies for their numerical solution are not necessarily straightforward, and techniques like the finite element method (FEM) have not yet been proven to be applicable. In addition, unlike integer-order stressdriven formulations that accept analytical solutions for selected cases [21,34], fractional-order governing equations very seldom allow for analytical solutions (especially when dealing with bounded domains). From a practical point of view, these aspects limit the need to explore stress-driven fractional-order formulations and suggest that their application to the analysis of structures having complex geometry and for general loading conditions would be more limited than its strain-based counterpart.

The remainder of the paper is structured as follows: first, we motivate the use of fractional calculus for the analysis of nonlocal structures by considering a 1D lattice with long-range interactions and its corresponding 1D continuum formulation. Next, we extend the 1D continuum to a fully 3D continuum and derive the governing equations in strong form using variational principles. Finally, we use the fractional-order formulation to analyze the effect of the fractional-order nonlocality on the static and free vibration response of beams and plates under different types of loading conditions.

2. Fractional-order mechanics: from lattice to 1D continuum

A well established route to develop formulations capable of capturing nonlocal effects in solids is to enforce the continuum limit on a lattice system whose particles are subject to long-range interactions. Several previous works have shown that the continuum limit of lattice structures with one-neighbour and two-neighbour interactions and constant interaction strength lead to the classical first and second integer-order straingradient theories of Mindlin, respectively [23,50]. An immediate extension of these models follows from considering the response of a lattice with even larger number (i.e. > 2) of long-range interactions. Assuming pair-wise constant interaction strengths between different masses across the lattice, it can be easily shown that higher integer-order strain-

gradient theories stem from these models. However, these integer-order strain-gradient models would invariably predict a stiffening response of the overall structure. Recall that both softening and stiffening responses have been experimentally observed in the response of solids sensitive to scale effects. In this study, we will show that fractional-order operators can offer a route to develop continuum models capable of predicting both softening and stiffening response in a single formulation. To obtain a physically consistent fractional-order continuum model, we start from a 1D lattice system in which particles are subject to long-range interactions whose pair-wise constant strength decreases with distance in a power-law fashion. While, in the past, other authors have modeled lattices with long-range cohesive forces using fractional calculus [38,39], in this study we extend the formulation by considering also the straingradient effects that arise due to microstructural considerations.

2.1. Lattice model and continualization procedure

Consider an infinite 1D lattice consisting of identical particles of mass M as shown in Fig. 1. The particles are periodically distributed in the \hat{x} direction with spatial period l_* and exhibit only longitudinal motion. The location and displacement of the nth particle (where $n \in \mathbb{Z}$) at the time t are denoted as $x_n(t)$ and $u_n(t)$, respectively. The strength of interaction between particles is modeled via lumped springs having stiffness $k_{i,j}$, where ith and jth are the two interacting particles and $i \neq j$. Note that, in this notation, the comma in the subscript of the spring stiffness does not indicate differentiation. In the following derivation, the dependence of u_i on time t will be implied. Using the above configuration of the lattice and assuming that all the springs are unstressed at the initial time t=0, the potential energy stored in the ith cell of the lattice is obtained as:

$$\mathcal{U}_{i} = \sum_{i=-\infty}^{\infty} \frac{1}{2} k_{i,j} |u_{i} - u_{j}|^{2} \tag{1}$$

where \mathcal{U}_i denotes the potential energy of the *i*th cell. By assuming small displacement gradients $(O(\varepsilon))$, Taylor's expansion at the point x_i gives:

$$u_i - u_j = (x_i - x_j)\delta_{x_j}^1 u_j + \frac{1}{2}(x_i - x_j)^2 \delta_{x_j}^2 u_j + h.o.t$$
 (2)

where $\delta_{x_j}^{\square}$ ($\square \in \{1,2\}$) denote the discretized integer-order derivatives at x_j .

It is well known that the strength of long-range cohesive forces decays as a function of the inter-atomic distance. Recall that, at continuum level and in integral formulations, this effect is typically accounted for by using convolution terms in the stress-strain constitutive relationships. These convolution kernels have often been chosen to be spatially-decaying exponential functions [12,20]. In the lattice model, the stiffness of the springs used to model the interaction between distant particles play a role analogous to the convolution kernels used in classical integral nonlocal elasticity. Thus, in principle, the stiffness of the springs emanating from a given particle towards distant particles can be modeled using spatially decaying exponential functions. In this study, we choose to model the stiffness spatial decay according to power-law functions as follows:

$$k_{i,j} = k_0 \left[\frac{c_1}{|x_{ij}|^{\alpha_1^2}} + \frac{c_2}{|x_{ij}|^{\alpha_2^2}} \right]$$
 (3)

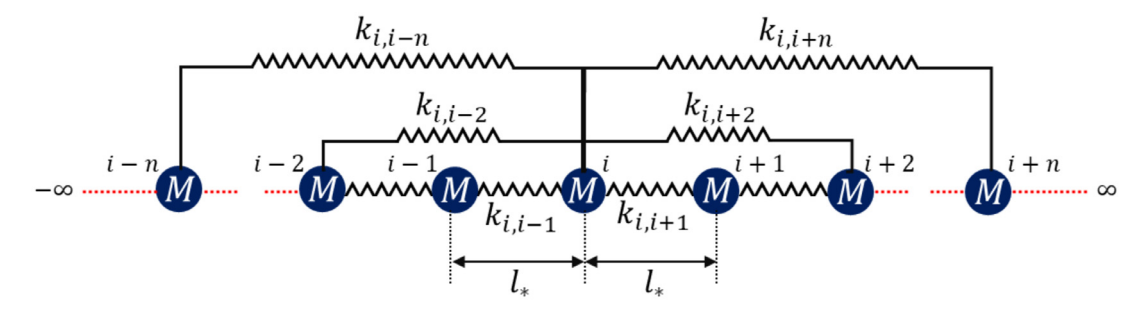


Fig. 1. Schematic of the infinite lattice consisting of identical masses denoted as M. The masses occur periodically in space separated by a distance of l. The schematic also illustrates the classical nearest-neighbour interactions as well the long-range interactions between the masses within the infinite lattice. Note that each mass within the lattice is connected to every other mass by spatially decaying long-range connections. To streamline the schematic, we have illustrated only the nonlocal connections of the mass M_i with a few other masses within the lattice.

where $|x_{ij}| = |x_i - x_j|$ indicates the distance between the *i*th and the *j*th particles. Note that the above equation is valid only for $i \neq j$, given that i = j would imply that the mass is connected to itself. The parameters α_1 and α_2 are such that $\alpha_1 \in (0, 1)$, $\alpha_2 \in (1, 2)$, and $\alpha_2 - \alpha_1 \in (0, 1)$. The specific reason behind choosing the aforementioned ranges for α_1 and α_2 is discussed later in this section with reference to the obtained continualized model. The coefficients c_1 and c_2 will be chosen as a function of the parameters α_1 and α_2 , respectively, such that they ensure dimensional consistency and frame-invariance of the formulation. Further, the constant k_0 has the dimensions of classical stiffness ($[MT^{-2}]$) and its physical significance will be discussed while deriving the continuum limit of the lattice. Note that the only parameters introduced at this level include α_1 , α_2 , and k_0 . For a given physical lattice with a known spatially decaying stiffness function, these parameters could be obtained by applying standard regression techniques. Substituting the expression of the stiffness in the infinite series in Eq. (1) along with Eq. (2) and retaining terms up to $O(\epsilon^2)$, we obtain the potential energy

$$U_{i} = \frac{k_{0}}{2} \left[\sum_{j=-\infty}^{\infty} \frac{\sqrt{c_{1}}(x_{i} - x_{j}) \delta_{x_{j}}^{1} u_{j}}{|x_{i} - x_{j}|^{\alpha_{1}}} \right]^{2} + \frac{1}{4} \left(\sum_{j=-\infty}^{\infty} \frac{\sqrt{c_{2}}(x_{i} - x_{j}) \delta_{x_{j}}^{2} u_{j}}{|x_{i} - x_{j}|^{\alpha_{2} - 1}} \right)^{2} \right]$$
(4)

By assuming a small l_* and adopting a continualization process similar to [23,50], the discrete variables indicating the position and the displacement of the particles, can be replaced by the corresponding continuum variables $(x_i \to x, x_j \to s, u_j \to u(s))$. The constant k_0 in the continuum limit can be defined as:

$$k_0 = \frac{EA}{l_*} \tag{5}$$

where E and A denote the Young's modulus and cross-sectional area of the equivalent 1D continuum, respectively. It follows that the constant k_0 can be interpreted as the equivalent spring constant representing the strength of the nearest-neighbor interaction forces of a lattice that simulate the microstructure of a local solid (that is not affected by scale effects). Further, we define the constants c_1 and c_2 in Eq. (3) as:

$$c_1 = \frac{l_*^2}{4\Gamma(1-\alpha_1)} \quad c_2 = \frac{l_*^4}{4\Gamma(2-\alpha_2)} \tag{6}$$

where $\Gamma(\cdot)$ denotes the Gamma function. Note that the interparticle interaction stiffness in Eq. (3) can be expressed directly without c_1 and c_2 , which can be treated as merely book keeping parameters. From a more mathematical perspective, the parameters c_1 and c_2 allow scaling the contributions of both the first and second derivatives of the displacement $(\delta^1_{x_j}u_j$ and $\delta^2_{x_j}u_j$, respectively) to the potential energy, hence providing a better control on their relative strength (see Eq. (4)).

Under the above assumptions, the continuum limit of the discrete sum in Eq. (4) is obtained to be the following integral representation

[51]

$$U(x) = \frac{EA}{2l_*} \left[I_*^2 \left[\frac{1}{2\Gamma(1-\alpha_1)} \int_{-\infty}^{\infty} \frac{D_s^1 u(s)}{|x-s|^{\alpha_1}} ds \right]^2 + \frac{I_*^4}{4} \left[\frac{1}{2\Gamma(2-\alpha_2)} \int_{-\infty}^{\infty} \frac{D_s^2 u(s)}{|x-s|^{\alpha_2-1}} ds \right]^2 \right]$$
(7)

where $D_s^m(\cdot)$ denotes the mth integer-order derivative with respect to the spatial dummy variable s used in the convolution integral. The convolution integrals in Eq. (7) match with the definition of fractional-order Caputo derivatives with intervals on the real axis, that is $x \in (-\infty, \infty)$ [52]:

$${}_{-\infty}^{C} D_{x}^{\alpha_{m}} u = \frac{1}{\Gamma(m - \alpha_{m})} \int_{-\infty}^{x} \frac{D_{s}^{m} u(s)}{(x - s)^{\alpha_{m} - m + 1}} ds$$
 (8a)

$${}_{x}^{C}D_{\infty}^{\alpha_{m}}u = \frac{(-1)^{m}}{\Gamma(m - \alpha_{m})} \int_{x}^{\infty} \frac{D_{s}^{m}u(s)}{(s - x)^{\alpha_{m} - m + 1}} ds$$
 (8b)

where $_{-\infty}^C D_x^{\alpha_m}(\cdot)$ denotes the left-handed Caputo derivative to the order α_m and lower terminal at $-\infty$, and $_x^C D_\infty^{\alpha_m}(\cdot)$ denotes the right-handed Caputo derivative to the order α_m and upper terminal at ∞ .

Using the above definitions of the left- and right-handed Caputo derivatives, the potential energy density at a point x can be expressed as:

$$\Pi(x) = \frac{U'(x)}{Al_*} = \frac{E}{2} \left[\left[\underbrace{\frac{1}{2} \left({_{-\infty}}^C D_x^{\alpha_1} u - {_{x}}^C D_{\infty}^{\alpha_2} u \right)}_{\text{Riesz-Caputo derivative}} \right]^2 + \underbrace{\frac{l_*^2}{4} \left[\underbrace{\frac{1}{2} \left({_{-\infty}}^C D_x^{\alpha_2} u + {_{x}}^C D_{\infty}^{\alpha_2} u \right)}_{\text{Riesz-Caputo derivative}} \right]^2} \right]$$

Recall that, from Eq. (3), $\alpha_1 \in (0, 1)$ and $\alpha_2 \in (1, 2)$. The above linear combinations of the left- and right-handed Caputo derivatives are typically referred to as the Riesz-Caputo (RC) derivatives. The total potential energy of the structure can now be expressed as:

$$\mathcal{U} = \int_{-\infty}^{\infty} \Pi(x) A dx = \frac{1}{2} \int_{-\infty}^{\infty} EA \left[\left(\overline{D}_x^{\alpha_1} u \right)^2 + \frac{l_*^2}{4} \left(\overline{D}_x^{\alpha_2} u \right)^2 \right] dx \tag{10}$$

where $\overline{D}_x^{u_m}(\cdot)$ denotes RC derivatives. The over bar $\overline{\ }$ is used to indicate that the RC derivative in Eq. (10) is defined on the real axis, so to differentiate the notation from the RC derivatives defined over bounded domains in Section 3. We merely note that the RC derivative used in the above equation is different from the concept of Riesz derivative defined using sets of Fourier and inverse Fourier transforms [52].

As evident from Eq. (10), the strain in the continuum limit of the infinite lattice structure subject to power-law decaying long-range interactions can be modeled using the RC derivative of the displacement field to the order $\alpha_1 \in (0, 1)$. The second term within the integral in Eq. (10) can be interpreted as the fractional-order gradient of the strain field. This is

evident by considering the following composition: $\overline{D}_x^{\alpha_2} u = \overline{D}_x^{\alpha_2 - \alpha_1} (\overline{D}_x^{\alpha_1} u)$. It follows that we could define a new order $\overline{\alpha}_2 = \alpha_2 - \alpha_1$. Recall that we have assumed $\alpha_2 - \alpha_1 \in (0,1)$ in Eq. (3). In order to avoid the introduction of new symbols, we will drop the overline and denote $\overline{\alpha}_2 \equiv \alpha_2$, with the understanding that α_2 now lies in the range (0,1). Thus, the total potential energy can be expressed as:

$$\mathcal{U} = \frac{1}{2} \int_{-\infty}^{\infty} EA \left[\left(\underbrace{\overline{D}_{x}^{\alpha_{1}} u}_{\text{Nonlocal strain}} \right)^{2} + \frac{l_{*}^{2}}{4} \left[\underbrace{\overline{D}_{x}^{\alpha_{2}} \left(\overline{D}_{x}^{\alpha_{1}} u \right)}_{\text{Nonlocal gradient of nonlocal strain}} \right]^{2} \right] dx$$
(11)

While the specific range for the fractional-orders mentioned here are obtained from mathematical definitions, we will obtain physical constraints on the range of these fractional-orders in Section 2.3.

Given the differ-integral nature of fractional operators, it appears that the different fractional-order derivatives in Eq. (11) lead to a unification of the classical integral and gradient based nonlocal approaches. In fact, the expression in Eq. (11) presents clear insights and comparisons of the fractional-order formulation with both the classical integral and the first-order strain-gradient formulation:

- The RC derivative with order α_1 captures softening effects in the solid due to the nonlocal interactions. The order α_1 captures the strength of the power-law kernel of the fractional derivative which in turn determines the rate of decay in the strength of the nonlocal interactions with distance. Further, the interval of the fractional derivative (here chosen to be $(-\infty,\infty)$), determines the length of the horizon of nonlocality. In other terms, it indicates the distance beyond which nonlocal interactions are no longer accounted for in the fractional derivative [7,45].
- From Eqs. (4)–(7) it is seen that, for the lattice with long-range cohesive interactions, the expression for the potential energy at a point x includes contribution of the microstructural information (that is the strain-gradient) of all points in the nonlocal horizon of x. This is in addition to the nonlocal contribution of the strain energy captured by the RC derivative $\overline{D}_x^{\alpha_1}u$. It is immediate to see that the RC derivative of the nonlocal strain with order α_2 captures the stiffening effects in the solid. More specifically, analogous to classical strain-gradient formulations, this term would account for the microstructural information within the strain energy potential. Furthermore, the parameter l_* that was initially introduced as the lattice parameter can be interpreted as the microstructural length scale analogously to classical formulations.

The above discussions lead to the conclusion that the use of the different fractional-order gradients allows the continuum model to capture simultaneously both long-range cohesive forces (leading to softening effects) as well as strain-gradient terms capturing microstructural properties (leading to stiffening effects). A remarkable outcome of this approach is that, not only it can capture both softening and stiffening effects in a single formulation, but it can account for these effects simultaneously. Note that the first-order strain-gradient theory for the 1D continuum can be obtained from the above formulation by using $\alpha_1 = 1$ and $\alpha_2 = 1$. Following the above discussion, we call α_1 as nonlocal-strain order and α_2 as the strain-gradient order.

The kinetic energy of the 1D solid can be evaluated similar to classical integer-order formulations. Note that the introduction of nonlocality through the long-range spring connections has no effect on the expression for kinetic energy. It follows that, in the continuum limit, the kinetic energy of the above described 1D solid is given as Metrikine and Askes [23], Polyzos and Fotiadis [50]:

$$T = \frac{1}{2} \int_{-\infty}^{\infty} \left[\rho A(D_t^1 u)^2 + \rho' A \frac{l_*^2}{3} \left[D_x^1 \left(D_t^1 u \right) \right]^2 \right] dx \tag{12}$$

where $D_l^1(\cdot)$ denotes the first integer-order derivative with respect to time, ρ is the density, and ρ' is the microdensity of the solid that has the

same interpretation as in classical integer-order strain-gradient models. A possible extension of the fractional-order continuum theory developed above involves the use of time fractional derivatives within the kinetic energy as:

$$T = \frac{1}{2} \int_{-\infty}^{\infty} \left[\rho A \binom{C}{0} D_t^{\kappa} u)^2 + \rho' A \frac{l_*^2}{3} \left[D_x^1 \binom{C}{0} D_t^{\kappa} u \right]^2 \right] dx$$
 (13)

where $_0^C D_i^\kappa u$ is a left-handed Caputo derivative with order $\kappa \in (0,1)$ and defined on the interval (0,t). This will allow the fractional-order model to capture memory effects and non-conservative dissipation mechanisms, such as those encountered in viscoelastic materials. Such a formulation can be found in Ansari et al. [53] where the nonlinear response of viscoelastic nanobeams have been captured by using time fractional derivatives. However, unlike our study, size-dependent effects in Ansari et al. [53] were modeled using the classical first-order strain-gradient formulation. Since memory effects and dissipation have already been addressed in the literature, in this study we focus on the modeling of nonlocal effects in non-dissipative solids using space fractional derivatives.

The above presented formulation deserves some additional remarks. First, the expression of the potential energy in Eq. (10) allows for an important remark on the range of the different fractional orders. It appears that, by adding additional higher-order power-law decaying terms (for example, $1/|x_{ij}|^{\alpha_3^2}$ with $\alpha_3 \in (2, 3)$) to the definition of the spring stiffness in Eq. (3), we can account for successive higher-order fractional strain gradients. As an example, upon including $1/|x_{ij}|^{\alpha_3^2}$, we would obtain the fractional-order equivalent of the classical second-order strain-gradient elasticity theory. In this study, we focused only on the fractional-order modification of the classical first-order strain-gradient formulation and hence, we have ignored higher-order power-law decaying terms in Eq. (3).

Second, note that the definition of the spring stiffness in Eq. (3) leads to $k_{i,j}=k_{j,i}$. This ensures that the internal state of the lattice cannot be changed following a translation of all the particles by the same distance. While this is sufficient to ensure frame-invariance of the 1D continuum, the extension to a full 3D model would require the satisfaction of frame-invariance under rotations as well. It is also important to note that the potential energy of the nonlocal 1D solid consists of Caputo derivatives and not other types of fractional derivatives (e.g. Riemann Liouville). Recall that the Caputo derivative of a constant function is zero, as for classical integer order derivatives. This property does not hold true for all definitions of fractional derivatives [52]. However, in the context of frame-invariance, this is a key point that ensures that no strain is accumulated in the 1D solid under translation, that is for a constant u(x).

Finally, we highlight that it is possible to envision different routes for the development of the fractional-order continuum model. As an example, a possible route to develop the fractional-order continuum formulation can start from more complex and higher-dimensional lattice structures similar to [54,55]. In such a case, the resulting fractionalorder continuum formulation would capture the information of additional lattice interactions via a higher number of material constants. It follows that the specific functional form of the fractional-order operator would be different from the definition adopted in this study (Eq. (9)). Nevertheless, the overall procedure to obtain the continuum limit of the lattice and all the subsequent analyses would still apply in an identical form. Hence, the general methodology presented in this study is applicable to other types of molecular models, provided that appropriate functional forms of the fractional operator are obtained. In this regard, we emphasize that the selected 1D lattice used in this study was intentionally chosen to yield a simplified mathematical structure, so to focus on the ability of the fractional-order operators to capture the long-range forces at molecular level as well as the microstructural properties in a cohesive and physically consistent manner.

2.2. Governing equations for the 1D continuum

We derive the dynamic governing equations of the 1D structure by using Hamilton's variational principle:

$$\int_{t_0}^{t_1} \delta(\mathcal{U} - T) dt = \int_{t_0}^{t_1} \delta \left[\frac{A}{2} \int_{-\infty}^{\infty} \left[E(\overline{D}_x^{\alpha_1} u)^2 + \frac{l_*^2}{4} E[\overline{D}_x^{\alpha_2} (\overline{D}_x^{\alpha_1} u)]^2 - \rho (D_t^1 u)^2 - \rho' \frac{l_*^2}{3} [D_x^1 (D_t^1 u)]^2 \right] dx dt$$
(14)

Performing variational simplifications, the governing equation is obtained as:

$$E\left[\overline{D}_{x}^{2\alpha_{1}}u - \frac{l_{*}^{2}}{4}\overline{D}_{x}^{2(\alpha_{1} + \alpha_{2})}u\right] = \rho D_{t}^{2}u - \rho' \frac{l_{*}^{2}}{3}D_{x}^{2}\left(D_{t}^{2}u\right) \tag{15}$$

A detailed derivation of the above equations is provided for a 3D bounded continuum in the Supplementary Information (SI).

Recall that capturing dispersive wave propagation is one of the main motivation promoting the development of gradient elasticity in classical elastodynamics. As discussed in detail in Askes and Aifantis [19], the use of "unstable" (integer-order) strain-gradients is critical in capturing wave dispersion, however, in the static sense, "unstable" straingradients result in non-convex potential energies leading to the loss of uniqueness in static boundary value problems (BVPs). In the classical analogue of Eq. (15), a positive (negative) sign of the strain-gradient term corresponds to an unstable (stable) strain-gradient. While the combined used of these gradient terms is generally avoided because one of the two terms will always tend to predominate, this issue is circumvented by using a combination of stable (integer-order) strain-gradients and acceleration gradients (see, Georgiadis et al. [22], Metrikine and Askes [23]) which allows for dispersive wave propagation while ensuring a well-posed BVP. A detailed discussion on this aspect can be found in Askes and Aifantis [19], where a combination of different stain and acceleration gradients¹ is studied to arrive at theories which are well suited for both static and dynamic applications. To this regard, we highlight that the fractional-order strain-gradient formulation provides a natural way of dealing with this issue without the need of additional stabilising acceleration gradients. Note that the potential energy given in Eq. (11), resulting from the fractional-order formulation, is quadratic in nature and hence fully convex. Additionally, it is established in Patnaik et al. [45] that the fractional-order operators are self-adjoint and the resulting formulation leads to well posed BVPs. Further, the specific form of the spring strength given in Eq. (3) indicates that the stiffness of the structure exhibits dependence on wavelength and hence, the fractional-order formulation, obtained via continualization of the Lagrangian of the 1D lattice, is well suited to capture anomalous dispersion characteristics (Section 2.3). Further, we will establish in the following Section 2.3 that the fractional-order formulation is causal and stable.

2.3. Dispersion analysis of the 1D continuum

To obtain the dispersion relation, we substitute in the fractionalorder elastodynamic equation given in Eq. (15) the following ansatz:

$$u(x,t) = u_0 e^{i(kx - \omega t)} \tag{16}$$

where u_0 is the amplitude of the longitudinal wave, k denotes the wavenumber, ω denotes the angular frequency of free longitudinal vibra-

tions, and $i = \sqrt{-1}$. For the RC derivatives on the real line used in Eq. (13) [52]:

$$D_{\nu}^{\alpha}(e^{kx}) = k^{\alpha}e^{kx} \tag{17}$$

Using the above RC derivative of the exponential, we obtain the complete form of the dispersion relations for longitudinal waves in the 1D solid as:

$$\frac{\omega}{k} = \sqrt{\frac{E}{\rho}} \left[-i^{2\alpha_1} k^{2(\alpha_1 - 1)} + i^{2(\alpha_1 + \alpha_2)} k^{2(\alpha_1 + \alpha_2 - 1)} \frac{l_*^2}{4} \right]^{\frac{1}{2}} \left[1 + \frac{\rho' l_*^2}{3\rho} k^2 \right]^{-1}$$
(18)

Using Euler's formula, the above equation can be recast in the following manner:

$$\frac{\omega}{k} = \mathcal{Z} = \left[\left(-\cos(\alpha_{1}\pi)k^{2(\alpha_{1}-1)} + \cos(2(\alpha_{1}+\alpha_{2})\pi)k^{2(\alpha_{1}+\alpha_{2}-1)}\frac{l_{*}^{2}}{4} \right) + i\left(-\sin(\alpha_{1}\pi)k^{2(\alpha_{1}-1)} + \sin(2(\alpha_{1}+\alpha_{2})\pi)k^{2(\alpha_{1}+\alpha_{2}-1)}\frac{l_{*}^{2}}{4} \right) \right]^{\frac{1}{2}}$$

$$\underbrace{\left[1 + \frac{\rho' l_{*}^{2}}{3\rho}k^{2} \right]^{-1}}_{\phi}$$
(19)

Expressing $\omega=\mathcal{Z}k$, stable and causal solutions are recovered when $\Re(\mathcal{Z})>0$ and $\Im(\mathcal{Z})<0$. Note from Eq. (16) that $\Re(\mathcal{Z})>0$ would lead to forward propagating solutions ensuring causality, while $\Im(\mathcal{Z})<0$ leads to attenuation hence ensuring stability. Thus, it appears that the complex number \mathcal{Z} must lie in the fourth quadrant of the Argand plane or, equivalently, \mathcal{Z}^2 must lie below the real-axis of the Argand plane. It immediately follows that the quantity $\bar{b}=\Im(\mathcal{Z}^2)$ in Eq. (18) must be less than or equal to zero for all values of k and l_* . The latter condition holds true for all positive values of the wave-number k and microstructural length l_* under the following restrictions for α_1 and α_2 :

$$\alpha_1, \alpha_2 \in [0.5, 1] \tag{20}$$

Under the above condition, $\sin{(\alpha_1\pi)}>0$ and $\sin{(2(\alpha_1+\alpha_2)\pi)}<0$, ensuring that $\bar{b}<0$ for all positive values of k and l_* . It follows that, in this study, we only consider values of the fractional-orders which lie in [0.5,1]. Under the above conditions, the $\Re(\mathcal{Z})$ would contribute to anomalous wave-number dependent dispersion in the propagating longitudinal waves while $\Im(\mathcal{Z})$ would lead to attenuation in the propagating waves.

Note that the term indicated by ϕ in Eq. (19) appears from the inclusion of the acceleration gradient term in the governing equations. As discussed in Askes and Aifantis [19], Sidhardh and Ray [56], the inclusion of the acceleration gradient term prevents an unbounded growth in the wave speed following an increase in the wave number. We merely note that, given the attenuation in the wave speed, the inclusion of the acceleration gradient term is no longer necessary in the fractional-order formulation. To this regard, note that ignoring the term ϕ would cause the dispersion as well as the attenuation in the longitudinal wave speeds to exhibit a power-law dependence on the wave-number. This is a direct consequence of the power-law nature of the strength of the long-range interactions. Remarkably, several studies have highlighted a power-law dependence of the attenuation-dispersion relations on frequency/wavenumber in many types of lossy and highly scattering media, including fractal and porous materials, and animal tissues [47-49]. It follows that, in this study, we will neglect the acceleration gradients and focus on modeling media with power-law attenuation-dispersion behavior. Another particularly interesting outcome of the above formulation is that the dispersion and attenuation form a Hilbert pair, ensuring that the dynamic formulation is fully causal [7,47,48].

¹ Different researchers have used different terminology (acceleration-gradient or velocity-gradient) to refer to the term $D_x^2(D_t^2u)$. We believe that both the terminology are appropriate since the term appears as an acceleration gradient in the strong form and translates to a velocity gradient in weak form. In this study, following [19], we refer to it as the acceleration gradient.

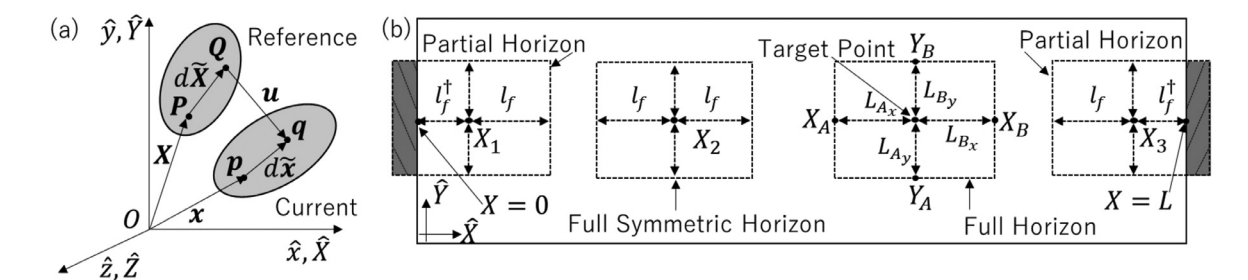


Fig. 2. (a) Schematic indicating the infinitesimal material $d\tilde{X}$ and spatial $d\tilde{x}$ line elements in the nonlocal medium subject to the displacement field u. (b) Horizon of nonlocality and length scales at three different material points X_1 , X_2 , and X_3 in a 2D domain. Note that in the \hat{X} direction, X_2 has a horizon of nonlocality equal to l_f on both the left and the right sides, while the horizon of nonlocality at the points X_1 and X_3 are truncated to l_f^{\dagger} such that $l_f^{\dagger} < l_f$, on the left and the right sides, respectively. Clearly, the nonlocal model can account for a partial (i.e. asymmetric) horizon condition that occurs at points close to a boundary or interface.

3. Extension to 3D continuum

The previous section used a 1D framework to illustrate the remarkable features of the fractional-order formulation. In this section, we extend the formulation to a fully three-dimensional and finite solid. The governing equations for the 3D continuum are derived using Hamilton's variational principle. We highlight here that, although the 3D formulation presented in the following is developed by continualization of the 1D lattice, the same formulation can also be derived from a continuummechanics approach by considering different configurations of a nonlocal solid, as illustrated in Patnaik and Semperlotti [7]. More specifically, the 3D formulation developed in this study via continualization principles can also be obtained from the fractional-order continuum formulation presented in Patnaik and Semperlotti [7] by adding fractional-order strain-gradient terms to the constitutive relations. To this regard, note that the continualization route adopted in this study motivates the need of a fractional-order approach to capture both stiffening and softening effects within a single formulation.

3.1. Weak formulation

The potential energy derived for the nonlocal 1D continuum in Eq. (11) is extended to a 3D continuum in the following manner:

$$\mathcal{U} = \frac{1}{2} \int_{\Omega} [\epsilon : C : \epsilon + \eta : G : \eta] dV$$
 (21)

where C denotes the classical fourth-order elasticity tensor and G is the sixth-order elasticity tensor. ϵ and η denote the fractional-order strain and its gradient, respectively. The volume of the 3D continuum is denoted by Ω and $d\mathbb{V}$ denotes an infinitesimal volume element. Note that the total potential energy is positive definite for positive definite material elasticity tensors.

The infinitesimal strain in the 3D nonlocal continuum is obtained by extending the 1D nonlocal strain indicated in Eq. (11) as:

$$\epsilon = \frac{1}{2} \left(\nabla^{\alpha_1} \boldsymbol{U}_X + \nabla^{\alpha_1} \boldsymbol{U}_X^T \right) = \frac{1}{2} \left(\nabla^{\alpha_1} \boldsymbol{u}_x + \nabla^{\alpha_1} \boldsymbol{u}_x^T \right)$$
 (22)

where U(X)=x(X)-X and u(x)=x-X(x) are the displacement fields in the Lagrangian (X) and Eulerian (x) coordinates, respectively (see Fig. 2(a)). $\nabla^{\alpha_m}(\cdot)$ $(\alpha_m \in \{\alpha_1,\alpha_2\})$ is the RC fractional gradient operator defined as:

$$\nabla^{\alpha_m}(\cdot) = D_x^{\alpha_m}(\cdot)\hat{x} + D_y^{\alpha_m}(\cdot)\hat{y} + D_z^{\alpha_m}(\cdot)\hat{z}$$
(23)

where $\{\hat{x}, \hat{y}, \hat{z}\}$ are the Cartesian basis vectors. $D_{x_j}^{\alpha_m}(\cdot)$ are the RC fractional derivatives which will be defined in the following. We emphasize that the above definition for the strain tensor can also be derived rigorously following a continuum mechanics approach, starting from a fractional-order definition of the deformation gradient tensor (see [7,45]). Further, the fractional gradient of the nonlocal strain is defined

as:

$$\eta = \nabla^{\alpha_2} \epsilon \tag{24}$$

It follows that the constitutive relations for the Cauchy stress and the higher-order stress, in terms of the work-conjugates ϵ and η , can be expressed as:

$$\sigma = C : \epsilon$$
 (25a)

$$\tau = G : \eta \tag{25b}$$

While the RC fractional derivatives used for the infinite 1D solid in Section 2 were defined on the real axis, these derivatives are modified for bounded domains to ensure frame-invariance everywhere on the domain and a complete kernel when approaching boundaries [7,45]. Note that completeness of the kernel in nonlocal elasticity is critical to ensure well-posed problems and stable numerical implementations. The space-fractional derivative $D_X^{\alpha_m}\psi(X,t)$ ($m\in\{1,2\}$) of the function $\psi(X,t)$ (= U(X,t) or $\epsilon(X,t)$) in Eqs. (22)–(24) is taken according to a RC definition with order $\alpha_m\in(0.5,1)$ defined on the interval $X\in(X_A,X_B)\in\mathbb{R}^3$. The RC definition for this bounded domain is defined as a linear combination of the left- and right-handed Caputo derivatives in the following manner [7]:

$$D_{\boldsymbol{X}}^{\alpha_{m}}\boldsymbol{\psi}(\boldsymbol{X},t) = \frac{1}{2}\Gamma(2-\alpha_{m})\left[L_{A}^{\alpha_{m}-1} X_{A}^{C} D_{\boldsymbol{X}}^{\alpha_{m}}\boldsymbol{\psi}(\boldsymbol{X},t) - L_{B}^{\alpha_{m}-1} X_{A}^{C} D_{\boldsymbol{X}_{B}}^{\alpha_{m}}\boldsymbol{\psi}(\boldsymbol{X},t)\right]$$
(26a)

$$D_{X_{j}}^{\alpha_{m}}\psi_{i}(\boldsymbol{X},t) = \frac{1}{2}\Gamma(2-\alpha_{m})\left[L_{A_{j}}^{\alpha_{m}-1} \sum_{X_{A_{j}}}^{C} D_{X_{j}}^{\alpha_{m}}\psi_{i}(\boldsymbol{X},t) - L_{B_{j}}^{\alpha_{m}-1} \sum_{X_{j}}^{C} D_{X_{B_{j}}}^{\alpha_{m}}\psi_{i}(\boldsymbol{X},t)\right]$$
(26b)

where, ${}_{X_A}{}^C D_X^{a_m} \psi(X,t)$ and ${}_X^C D_{X_B}^{a_m} \psi(X,t)$ are the left- and right-handed Caputo derivatives of $\psi(X,t)$ respectively. In the indicial expression in Eq. (26b), L_{A_j} and L_{B_j} are length scales along the jth direction in the reference configuration. The index j in Eq. (26b) is not a repeated index because the length scales are scalar multipliers. In the current configuration, these length scales are denoted as l_{A_j} and l_{B_j} . The interval of the fractional derivative (X_A, X_B) defines the horizon of nonlocality which is schematically shown in Fig. 2 for a generic point $X \in \mathbb{R}^2$. This interval defines the set of all points in the solid that influence the elastic response at X or, equivalently, the characteristic distance beyond which information of nonlocal interactions is no longer accounted for in the derivative.

Recall that the use of Riesz-Caputo derivatives ensured a frame-invariant model for the 1D continuum. The analysis of frame-invariance is necessary for the fractional-order approach because the integration of the nonlocal behavior occurs via the kinematic (strain-displacement) relations (see Eq. (22)). Under this assumption, frame-invariance is not automatically guaranteed. This is contrary to integer-based approaches

to nonlocal elasticity (regardless if in strain- or stress-driven form) which are based on a classical continuum mechanics framework and therefore, automatically satisfy the concept of frame-invariance in a classical sense. Thus, it is essential to establish that the state of stress is not altered by rigid body motions of either the solid or of any observer. The frame invariance was rigorously established in Patnaik and Semperlotti [7] where it was shown that either a rigid rotation or translation of the solid does not alter the state of strain (or stress) in the solid. As discussed in Patnaik and Semperlotti [7], the terms $\frac{1}{2}\Gamma(2-\alpha_m)$, $L_{A_i}^{\alpha_m-1}$, and $L_{B}^{\alpha_m-1}$ are critical to ensure the frame-invariance of the 3D formulation. Further, the length scales must satisfy the conditions $L_A = X - X_A$ and $L_B = X_B - X$. Hence, it follows that the length scales, L_A , and L_B physically denote the dimension of the horizon of nonlocality to the left and to the right of a point X along the jth direction. The length scales have been schematically illustrated in Fig. 2(b). The introduction of the different length scales (L_A and L_B) also enables the formulation to deal with possible asymmetries in the horizon of nonlocality (e.g. resulting from a truncation of the horizon when approaching a boundary or an interface). Note also that the length scale parameters ensure the dimensional consistency of the formulation.

A key aspect in nonlocal integral formulations is the nature of the kernel when approaching the boundaries. To this regard, we highlight that the definition of the RC derivative in Eq. (26) ensures the completeness of the power-law convolution kernel within the fractional-order derivative. Note that the lower terminal is $X_A = X - L_A$ and the upper terminal is $X_B = X + L_B$. This definition allows the length scales L_A and L_B to be truncated when the point X approaches a boundary (see Fig. 2(b)). It follows that the terminals of the RC derivative are properly modified hence resulting in a complete kernel over the truncated domain. We highlight that this truncation of the terminal of the RC derivative (or, the horizon of nonlocality) is analogous to the modification of the potential energy in lattice mechanics, where contributions from missing bonds for atoms close to boundaries are removed [55].

The completeness of the kernel can also be established by investigating the nature of the fractional-order model at points on the boundary, that is when either $L_{A_j} \to 0$ or $L_{B_j} \to 0$. As established in Patnaik and Semperlotti [7], Patnaik et al. [45], for a material point (say \textbf{X}_0) located on one of the boundaries (identified by the normal in the jth direction), for the limiting case when $L_{A_j} \to 0$, the RC fractional derivative reduces to:

$$\lim_{L_{A_{j}}\to 0} D_{X_{j}}^{\alpha_{m}} \psi_{i}(\boldsymbol{X}, t) \tag{27}$$

$$= \frac{1}{2} \left[\underbrace{\frac{\mathrm{d}\psi_{i}(\boldsymbol{X}, t)}{\mathrm{d}X_{j}} \bigg|_{X_{0}}}_{\text{Local effect due to truncation of nonlocal horizon}} + \underbrace{(1 - \alpha_{m}) L_{B_{j}}^{\alpha_{m}-1} \int_{X_{0_{j}}}^{X_{B_{j}}} \frac{D_{S_{j}}^{1} \psi_{i}(\boldsymbol{S}, t)}{(S_{j} - X_{j})^{\alpha_{m}}} dS_{j}} \right]}_{\text{Remaining nonlocal interactions}}$$

$$\underset{\text{Removal of non-existing bond energies}}{\text{Remaining nonlocal interactions}}$$

where S_j is a dummy vector variable used to carry out the spatial convolution integral. From Eq. (27) it is immediate to observe that while the right-handed Caputo derivative captures nonlocality ahead of the point X_0 (in the jth direction), the left-handed derivative is reduced to the classical first-order derivative. This result suggests that the truncation of the nonlocal horizon (and the corresponding convolution) at the boundary has been accounted for in a consistent manner analogous to the approach used in molecular models [55]. Similar expressions hold when $L_{B_i} = 0$ and for the deformed configuration ($l_{A_i} = 0$ or $l_{B_i} = 0$).

The above discussions on the frame-invariance of the formulation and on the nature of the kernel close to material boundaries establish both the completeness and consistency of the fractional-order continuum formulation. It remains to obtain the expressions for the kinetic energy of the continuum and the work done by externally applied forces. The work done by external forces is defined analogous to classical for-

mulations of gradient elasticity as:

$$\mathcal{V} = \int_{\Omega} (\overline{\boldsymbol{b}} \cdot \boldsymbol{u}) d\mathbb{V} + \int_{\partial \Omega} (\overline{\boldsymbol{t}} \cdot \boldsymbol{u} + \overline{\boldsymbol{q}} \cdot \hat{\boldsymbol{n}} \cdot (\boldsymbol{u} \otimes \nabla^{\alpha_1})) d\mathbb{A} + \oint_{\overline{\Gamma}} (\overline{\boldsymbol{r}} \cdot \boldsymbol{u}) dl$$
(28)

where dA and dl indicate area and line elements along the surface $\partial\Omega$ (with normal \hat{n}) and edge $\overline{\Gamma}$ of the solid, respectively. The bar on $\overline{\Gamma}$ symbol in the above equation, is used to differentiate the same from the $\Gamma(\cdot)$ function and the symbol \otimes denotes the dyadic product. \bar{b} , \bar{t} , \bar{q} , and \bar{r} are the prescribed values of body force per unit volume, surface traction per unit area, double stress traction vector and line load along sharp edges of the continuum, respectively. Finally, recalling that the introduction of nonlocality has no effect on the expression of the kinetic energy, we can write:

$$T = \frac{1}{2} \int_{\Omega} \rho(\dot{\boldsymbol{u}} \cdot \dot{\boldsymbol{u}}) dV \tag{29}$$

where ρ indicates the density of the solid and \Box indicates the first integer-order derivative with respect to time. By using the Hamilton's principle and the expressions of the potential energy, kinetic energy, and work done by external forces, the weak form of the governing equations for the 3D continuum are expressed as:

$$\int_{t_1}^{t_2} (\delta \mathcal{U} - \delta V - \delta T) dt = 0$$
(30)

3.2. Strong formulation

The strong form of the fractional-order governing equations are obtained by applying the fundamental law of variational calculus to Eq. (30). Analogously to classical integer-order formulations, the procedure to obtain the strong form for 3D domains involves the use of different principles of vector calculus. To this regard, note that fractional vector calculus principles have been recently developed and do not hold true for a general bounded geometry [57]. This aspect can be attributed to the fact that fractional-order operators (i.e. derivatives or integrals) do not generally commute, except when defined on the real axis [52,57]. However, we will show that the variational statement in Eq. (30) can be exactly simplified when considering a cuboidal (or, rectangular) geometry. It can also be envisioned that, the strong form derived assuming a cuboidal geometry will also be applicable for geometries wherein the surfaces/edges can be exactly represented or even approximated by using rectangular/line elements. Although the strong form requires the simplified cuboidal geometry, we emphasize that the weak form in Eq. (30) is applicable to any geometry.

Considering the cuboidal geometry Ω illustrated in Fig. 3, the first variation of the potential energy is obtained as:

$$\begin{split} \delta \mathcal{U} &= -\int_{\Omega} \widetilde{\nabla}^{\alpha_{1}} \cdot \left(\sigma - \widetilde{\nabla}^{\alpha_{2}} \cdot \tau \right) \cdot \delta \mathbf{u} \mathrm{d} \mathbb{V} + \int_{\partial \Omega} \left[\boldsymbol{I}_{\hat{\boldsymbol{n}}}^{1-\alpha_{1}} \cdot \left(\sigma - \widetilde{\nabla}^{\alpha_{2}} \cdot \tau \right) \right. \\ &\left. - \left[\boldsymbol{R} : \left(\boldsymbol{I}_{\hat{\boldsymbol{n}}}^{1-\alpha_{2}} \cdot \tau \right) \otimes \widetilde{\nabla}^{\alpha_{1}} \right] \right] \cdot \delta \mathbf{u} \mathrm{d} \mathbb{A} + + \int_{\partial \Omega} \left[\boldsymbol{I}_{\hat{\boldsymbol{n}}}^{1-\alpha_{2}} \otimes \hat{\boldsymbol{n}} \right] : \tau \\ &\left. \cdot \left[\hat{\boldsymbol{n}} \cdot \left(\delta \mathbf{u} \otimes \nabla^{\alpha_{1}} \right) \right] \mathrm{d} \mathbb{A} + \oint_{\widetilde{\Gamma}} \left[\left[\boldsymbol{I}_{\hat{\boldsymbol{n}}}^{1-\alpha_{1}} \cdot \left(\boldsymbol{I}_{\hat{\boldsymbol{n}}}^{1-\alpha_{2}} \cdot \tau \right) \right] \right] \cdot \delta \mathbf{u} \mathrm{d} \mathbf{l} \end{split}$$
(31)

The detailed derivation of the above governing equations is provided in the SI. In Eq. (31), the tensor R is the projector onto the surface $\partial\Omega$, \hat{m} is the co-normal vector at the edges and $[[\,\cdot\,\,]]$ operator denotes difference of the argument across both sides of the edge $\overline{\Gamma}$. For smooth edges (for example, a cube with filleted edges), the line integral vanishes analogous to classical formulations [58]. R and \hat{m} are given as:

$$R = 1 - \hat{n} \otimes \hat{n} \tag{32a}$$

$$\hat{\boldsymbol{m}} = \hat{\boldsymbol{s}} \wedge \hat{\boldsymbol{n}} \tag{32b}$$

where \hat{s} is a unit vector tangent to the edge $\overline{\Gamma}$ and \wedge denotes the exterior product. The operator $I_h^{1-\alpha_m}(\cdot)$ is defined as:

$$I_{\hat{n}}^{1-\alpha_{m}}(\cdot) = n_{x} I_{x}^{1-\alpha_{m}}(\cdot)\hat{x} + n_{y} I_{y}^{1-\alpha_{m}}(\cdot)\hat{y} + n_{z} I_{z}^{1-\alpha_{m}}(\cdot)\hat{z}$$
(33)

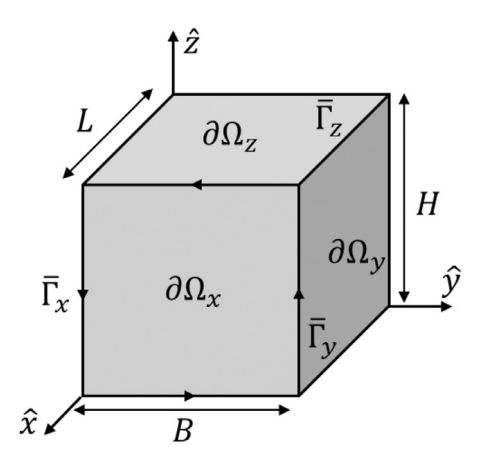


Fig. 3. Schematic of the cuboidal domain (Ω) illustrating the different geometrical parameters. The surface of the cuboid is given as $\partial\Omega=\partial\Omega_x\cup\partial\Omega_y\cup\partial\Omega_z$, where $\partial\Omega_{x_k}$ denotes a surface with its normal oriented along the positive or negative \hat{x}_k axis. The edges of the cuboid are denoted by $\overline{\Gamma}=\overline{\Gamma}_x\cup\overline{\Gamma}_y\cup\overline{\Gamma}_z$. $\overline{\Gamma}_{x_k}$ denotes the edges of the surface $\partial\Omega_{x_k}$ oriented in the anti-clockwise sense with respect to the normal to the surface.

such that $\hat{\mathbf{n}} = n_x \hat{x} + n_y \hat{y} + n_z \hat{z}$. The same definition directly extends to the operator $I_{\hat{m}}^{1-\alpha_m}(\cdot)$ that appears in Eq. (31). Further, $I_{x_j}^{1-\alpha_m}(\cdot)$ is a Riesz integral operator defined in the following manner:

$$I_{x_{j}}^{1-\alpha_{m}}\chi = \frac{1}{2}\Gamma(2-\alpha_{m})\left[I_{B_{j}}^{\alpha_{m}-1}\binom{1}{x_{j}-l_{B_{j}}}I_{x_{j}}^{1-\alpha_{m}}\chi\right) + I_{A_{j}}^{\alpha_{m}-1}\binom{1}{x_{j}}I_{x_{j}+l_{A_{j}}}^{1-\alpha_{m}}\chi\right]$$
(34)

where $x_1=x,\,x_2=y$ and $x_3=z.\,_{x_j-l_{B_j}}I_{x_j}^{1-\alpha_m}\chi$ and $_{x_j}I_{x_j+l_{A_j}}^{1-\alpha_m}\chi$ are the left and right Riesz integrals (in the x_j direction) to the order α_m of an arbitrary function χ . Further, the gradient operator denoted by $\widetilde{\nabla}^{\alpha_m}(\cdot)$ is a Riesz Riemann-Liouville gradient (analogous to the RC gradient $\nabla^{\alpha_m}(\cdot)$ in Eq. (23)) containing Riesz Riemann-Liouville derivatives instead of RC derivatives. More specifically,

$$\widetilde{\nabla}^{\alpha_m}(\cdot) = \mathfrak{D}_{\nu}^{\alpha_m}(\cdot)\hat{x} + \mathfrak{D}_{\nu}^{\alpha_m}(\cdot)\hat{y} + \mathfrak{D}_{\tau}^{\alpha_m}(\cdot)\hat{z}$$
(35)

where $\mathfrak{D}_{x_j}^{a_m}(\cdot)$ is the Riesz Riemann-Liouville derivative of order a_m which is defined as:

$$\mathfrak{D}_{x_{j}}^{\alpha_{m}} \chi = \frac{1}{2} \Gamma(2 - \alpha_{m}) \left[l_{B_{j}}^{\alpha_{m} - 1} \binom{RL}{x_{j} - l_{B_{j}}} D_{x_{j}}^{\alpha_{m}} \chi \right) - l_{A_{j}}^{\alpha_{m} - 1} \binom{RL}{x_{j}} D_{x_{j} + l_{A_{j}}}^{\alpha_{m}} \chi \right]$$
(36)

where ${}_{x_j-l_{B_j}}^{RL} \mathcal{D}_{x_j}^{\alpha_m} \chi$ and ${}_{x_j}^{RL} \mathcal{D}_{x_j+l_{A_j}}^{\alpha_m} \chi$ are the left- and right-handed Riemann Liouville derivatives of χ to the order α_m , in the x_j direction. Note that the Riesz fractional derivative $\mathfrak{D}_{x_j}^{\alpha_m}(\cdot)$ and the Riesz fractional integral $I_{x_j}^{1-\alpha_m}(\cdot)$ are defined over the interval $(x_j-l_{B_j},x_j+l_{A_j})$ unlike the RC fractional derivative $\mathcal{D}_{x_j}^{\alpha_m}(\cdot)$ which is defined over the interval $(x_j-l_{A_j},x_j+l_{B_j})$. This change in the terminals of the interval of the Riesz Riemann-Liouville integral and derivative follows from the variational simplifications (see SI).

The first variation of the external work done follows directly from Eq. (28) as:

$$\delta \mathcal{V} = \int_{\Omega} (\overline{\boldsymbol{b}} \cdot \delta \boldsymbol{u}) d\mathbb{V} + \int_{\partial \Omega} (\overline{\boldsymbol{t}} \cdot \delta \boldsymbol{u} + \overline{\boldsymbol{q}} \cdot \hat{\boldsymbol{n}} \cdot (\delta \boldsymbol{u} \otimes \nabla^{\alpha_1})) d\mathbb{A} + \oint_{\Gamma} (\overline{\boldsymbol{r}} \cdot \delta \boldsymbol{u}) d\mathbb{I}$$
(37)

Further, the first variation of the kinetic energy is obtained as:

$$\delta T = -\int_{\Omega} \rho \ddot{\mathbf{u}} \cdot \delta \mathbf{u} d\mathbb{V} \tag{38}$$

Now by using the extended Hamilton's principle in Eq. (30) and applying the fundamental theorem of variational calculus, the elastodynamic governing equations for the 3D nonlocal continuum are obtained as:

$$\widetilde{\nabla}^{\alpha_1} \cdot (\boldsymbol{\sigma} - \widetilde{\nabla}^{\alpha_2} \cdot \boldsymbol{\tau}) + \overline{\boldsymbol{b}} = \rho \ddot{\boldsymbol{u}} \quad \forall \ \boldsymbol{x} \in \Omega$$
(39)

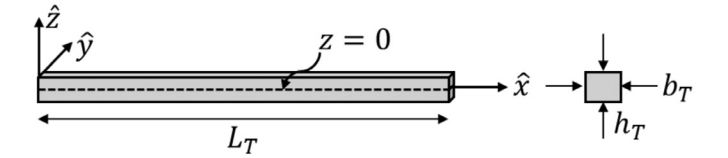


Fig. 4. Schematic of the beam illustrating the different geometric parameters.

The associated boundary conditions are obtained as:

$$I_{\hat{n}}^{1-\alpha_{1}}\cdot\left(\sigma-\widetilde{\nabla}^{\alpha_{2}}\cdot\tau\right)-\left[R:\left(I_{\hat{n}}^{1-\alpha_{2}}\cdot\tau\right)\otimes\widetilde{\nabla}^{\alpha_{1}}\right]=\overline{t}\quad\text{or}\quad u=\overline{u}\quad\forall\ x\in\partial\Omega$$
(40a)

$$\left[\boldsymbol{I}_{\hat{\boldsymbol{n}}}^{1-\alpha_2} \otimes \boldsymbol{n} \right] : \boldsymbol{\tau} = \overline{\boldsymbol{q}} \quad \text{or} \quad \hat{\boldsymbol{n}} \cdot (\delta \boldsymbol{u} \otimes \boldsymbol{\nabla}^{\alpha_1}) = \hat{\boldsymbol{n}} \cdot (\delta \overline{\boldsymbol{u}} \otimes \boldsymbol{\nabla}^{\alpha_1}) \quad \forall \ \boldsymbol{x} \in \partial\Omega \tag{40b}$$

$$\left[\left[I_{\hat{n}}^{1-\alpha_{1}}\cdot\left(I_{\hat{n}}^{1-\alpha_{2}}\cdot\boldsymbol{\tau}\right)\right]\right]=\overline{\boldsymbol{r}}\quad\text{or}\quad\boldsymbol{u}=\overline{\boldsymbol{u}}\quad\forall\;\boldsymbol{x}\in\overline{\boldsymbol{\Gamma}}\tag{40c}$$

Note that the natural boundary conditions are nonlocal in nature. This is similar to what is seen in classical integral approaches [3,12]. The nonlocal nature follows from the nonlocal definition of the constitutive relations given in Eq. (25). It follows that the surface tractions depend on the response of a range of particles, hence leading to nonlocal boundary conditions. The partial horizon at the point X_3 in Fig. 2) serves as an example to illustrate the nonlocal nature of the boundary condition. We anticipate that the nonlocal nature of the natural boundary conditions does not concern us immediately as we will solve the above system of equations using a finite element (FE) technique. Recall that natural boundary conditions are implicitly satisfied when obtaining the solutions using FE techniques and are accurate up to the order of the specific finite element. Additionally, the following initial conditions are required to obtain the transient response:

$$\delta \mathbf{u} = 0 \quad \text{and} \quad \delta \dot{\mathbf{u}} = 0 \quad \forall \ \mathbf{x} \in \Omega \text{ at } t = 0$$
 (41)

Given the complex nature of the fractional-order governing equations and the associated boundary conditions, they do not generally admit closed-form analytical solutions. Consequently, numerical methods become indispensable to simulate the above governing equations. This issue is typical also of classical strain-gradient or integral nonlocal approaches, which typically are solved via numerical techniques [19].

In the following, we will use the fractional-order continuum formulation developed above to analyze both the static and the free vibration response of slender nonlocal structures, including a Timoshenko beam and a Mindlin plate. We will demonstrate that the fractional-order continuum model is able to capture both stiffening and softening effects depending on the values of the parameters involved in the fractional formulation. Numerical solutions will be obtained by using an adapted version of the fractional-order FEM (f-FEM) developed in Patnaik et al. [44], 45] for fractional-order nonlocal BVPs. Note that the f-FEM is obtained by discretization of the Hamiltonian of the system using an isoparametric formulation. Hence, we only provide the weak form of the governing equations for the Timoshenko beam and the Mindlin plate. The strong form of the governing equations for both the beam and the plate can be easily obtained following the detailed derivation of the 3D governing equations outlined in the SI.

4. Application to Timoshenko beams

We start analyzing the fractional-order continuum model by considering its application to a Timoshenko beam. A schematic of the undeformed beam along with the chosen Cartesian reference frame is illustrated in Fig. 4. The top surface of the beam is identified as $z = h_T/2$, while the bottom surface is identified as $z = -h_T/2$. The width of the beam is denoted as b_T . The domain corresponding to the mid-plane of the beam (i.e., z = 0) is denoted as Ω_T , such that $\Omega_T = [0, L_T]$ where

 L_T is the length of the beam. The domain of the beam is identified by the tensor product $\Omega_T \otimes [-b_T/2, b_T/2] \otimes [-h_T/2, h_T/2]$. The subscript T indicates that all the above dimensions correspond to the Timoshenko beam.

For the Timoshenko beam, analogous to the classical case, the axial and transverse components of the displacement field denoted by u(x, y, z, t) and w(x, y, z, t) at any spatial location x(x, y, z) are related to the mid-line displacements of the beam in the following manner:

$$u(x, y, z, t) = u_0(x, t) - z\theta_0(x, t)$$
 (42a)

$$w(x, y, z, t) = w_0(x, t) \tag{42b}$$

where u_0 and w_0 are the mid-plane axial and transverse displacements of the beam, and θ_0 is the rotation of the transverse normal of the beam about the \hat{y} axis. In the following, for a compact notation, the functional dependence of the displacement fields on the spatial and the temporal variables will be implied unless explicitly expressed to be constant. Based on the above displacement fields, the non-zero strain components in the Timoshenko beam are evaluated using Eq. (22) as:

$$\epsilon_{xx} = D_x^{\alpha_1} u_0 - z D_x^{\alpha_1} \theta_0 \tag{43a}$$

$$\epsilon_{xz} = \frac{1}{2} \left[D_x^{\alpha_1} w_0 - \theta_0 \right] \tag{43b}$$

The strain-gradients developed in the beam are obtained using Eq. (24) as:

$$\eta_{xxr} = D_r^{\alpha_2} \left[D_x^{\alpha_1} u_0 - z D_x^{\alpha_1} \theta_0 \right] \tag{44a}$$

$$\eta_{xzr} = D_r^{a_2} \left[\frac{1}{2} \left[D_x^{a_1} w_0 - \theta_0 \right] \right] \tag{44b}$$

where $r \in \{x, y, z\}$. Specializing the above expressions, the following strain-gradient components are obtained exactly:

$$\eta_{xxz} = D_z^{\alpha_2} \left[D_x^{\alpha_1} u_0 \right] - D_z^{\alpha_2} \left[z D_x^{\alpha_1} \theta_0 \right] = -D_x^{\alpha_1} \theta_0 \tag{45a}$$

$$\eta_{xzx} = \frac{1}{2} \left[D_x^{\alpha_2} \left[D_x^{\alpha_1} w_0 \right] - D_x^{\alpha_2} \theta_0 \right] = -\frac{1}{2} D_x^{\alpha_2} \theta_0 \tag{45b}$$

$$\eta_{xzz} = \frac{1}{2} \left[D_z^{\alpha_2} \left[D_x^{\alpha_1} w_0 \right] - D_z^{\alpha_2} \theta_0 \right] = 0 \tag{45c}$$

In the above simplification we have used that $D_z^{\alpha_2}[z]=1$, which is exact and follows immediately from the definition of the RC derivative defined in Eq. (26). Further, assuming small displacement gradients ($O(\epsilon)$), the strain-gradient η_{xxx} is $O(\epsilon^2)$ while the strain-gradients in Eq. (45) are either $O(\epsilon)$ or exactly zero. Hence it appears that, for the normal strain ϵ_{xx} , the transverse strain-gradient η_{xxx} is significant when compared to the axial gradient η_{xxx} . Conversely, for the shear strain ϵ_{xz} , the axial gradient η_{xxx} is significant while the transverse gradient η_{xzz} is exactly zero. Thus, when obtaining the response of the beam via the weak form, the contribution of the strain-gradient η_{xxx} can be ignored when compared to the contribution of the non-zero strain-gradients in Eq. (45). We have further justified this approximation in detail in the SI.

The first variations of the nonlocal potential energy, the work done by externally applied forces, and the kinetic energy corresponding to the Timoshenko beam assumptions are obtained as:

$$\begin{split} \delta \mathcal{U} &= \int_0^{L_T} \left[N_{xx} \delta D_x^{\alpha_1} u_0 + M_{xx} \delta D_x^{\alpha_1} \theta_0 + Q_{xz} \delta (D_x^{\alpha_1} w_0 - \theta_0) \right. \\ &\left. + \overline{N}_{xxz} \delta D_x^{\alpha_1} \theta_0 + \overline{N}_{xzx} \delta D_x^{\alpha_2} \theta_0 \right] \mathrm{d}x \end{split} \tag{46a}$$

$$\delta \mathcal{V} = \int_{0}^{L_{T}} \int_{-\frac{b_{T}}{2}}^{\frac{b_{T}}{2}} \int_{-\frac{h_{T}}{2}}^{\frac{h_{T}}{2}} \left[F_{x} \delta u_{0} + F_{z} \delta w_{0} + M_{\theta_{0}} \delta \theta_{0} \right] dz dy dx \tag{46b}$$

$$\delta T = \int_0^{L_T} \int_{-\frac{b_T}{2}}^{\frac{b_T}{2}} \int_{-\frac{h_T}{2}}^{\frac{h_T}{2}} \rho \left[\left(\dot{u}_0 - z \dot{\theta}_0 \right) \left(\delta \dot{u}_0 - z \delta \dot{\theta}_0 \right) + \dot{w}_0 \delta \dot{w}_0 \right] dz dy dx \quad (46c)$$

 $\{F_x, F_z\}$ are the external loads applied in the axial (\hat{x}) and transverse (\hat{z}) directions, respectively, and M_{θ_0} is the external moment applied about the \hat{y} axis. The axial stress resultant $\{N_{xx}\}$, the shear resultant $\{Q_{xz}\}$, the moment resultant $\{M_{xx}\}$, and the higher-order stress resultants $\{\overline{N}_{xx}, \overline{N}_{xx}\}$ in Eq. (46a) are given as:

$$\begin{aligned} &\{N_{xx},Q_{xz},M_{xx},\overline{N}_{xxz},\overline{N}_{xzx}\}\\ &=\int_{-\frac{b_T}{2}}^{\frac{b_T}{2}}\int_{-\frac{b_T}{2}}^{\frac{b_T}{2}}\{\sigma_{xx},K_s\sigma_{xz},-z\sigma_{xx},-\tau_{xxz},-K_s\tau_{xzx}\}\mathrm{d}z\mathrm{d}y \end{aligned} \tag{47}$$

where K_s is the shear correction factor.

In the following, we briefly discuss the f-FEM method used to numerically simulate the fractional-order system. The details of the f-FEM are extensive and will not be reported here, but the interested reader can refer to [44,45]. The f-FEM for the Timoshenko beam is formulated by obtaining a discretized form of the first variation of the Lagrangian of the beam. For this purpose, the beam domain $\Omega_T = [0,L]$ is uniformly discretized into disjoint three-noded line elements and the different fractional derivatives that appear in Eq. (46a) are expressed as:

$$D_x^{\alpha_1} \left[u_0(x) \right] = \left[\tilde{B}_{u_0, x}^{\alpha_1}(x) \right] \{ U \} \tag{48a}$$

$$D_x^{\alpha_m} \left[\theta_0(x) \right] = \left[\tilde{B}_{\theta_0, x}^{\alpha_m}(x) \right] \{ U \} \tag{48b}$$

$$D_x^{\alpha_1} \left[w_0(x) \right] - \theta_x = \left[\left[\tilde{B}_{w_0,x}^{\alpha_1}(x) \right] - \left[\mathbb{L}^{(\theta_0)}(x) \right] \right] \left\{ U \right\} \tag{48c}$$

where $\{U\}$ denotes the global degrees of freedom vector and $[\mathbb{L}^{(\theta_0)}(x)]$ is obtained by assembling the element interpolation vectors for θ_0 . The matrices $[\tilde{B}^{a_m}_{\square x}(x)]$ contain the fractional-order derivatives of the shape functions used to interpolate the nodal displacement degrees of freedom of the Timoshenko beam. A brief discussion on the details of these matrices is provided in SI. By using the above expressions for the FE approximation of the different fractional-order derivatives, the first variation of the potential energy $\delta \mathcal{U}$ given in Eq. (46a) is obtained as:

$$\delta \mathcal{U} = \delta \{U\}^T \left[\int_{\Omega_T} [\tilde{B}_T(x)]^T [S_T] [\tilde{B}_T(x)] d\Omega_T \right] \{U\} = \delta \{U\}^T [K_T] \{U\} \quad (49)$$

where $[S_T]$ is the constitutive matrix of the beam and $[\tilde{B}_T(x)]$ is given as:

$$[\tilde{B}_T(x)] = \underbrace{\left[\underbrace{\tilde{B}_{u_0,x}^{a_1}(x)}\right]^T, \left[[\tilde{B}_{u_0,x}^{a_1}(x)] - [\mathbb{L}^{(\theta_0)}(x)]\right]^T}_{\text{Contributions from the nonlocal strains}}, \underbrace{\left[\underbrace{\tilde{B}_{\theta_0,x}^{a_1}(x)}\right]^T, \left[\tilde{B}_{\theta_0,x}^{a_2}(x)\right]^T, \left[\tilde{B}_{\theta_0,x}^{a_2}(x)\right]^T}_{\text{Contributions from the nonlocal strain-gradients}}\right]^T}$$

The algebraic equations for the f-FEM are given as:

$$[M_T]\{\ddot{U}\} + [K_T]\{U\} = \{F_T\} \tag{51}$$

where the stiffness matrix $[K_T]$ is indicated in Eq. (49). The expressions for the force vector $\{F_T\}$ and the mass matrix $[M_T]$ follow directly from classical Timoshenko beam formulations and are provided in SI. The solution of the algebraic Eq. (51) gives the nodal displacement variables which can then be used along with the kinematic relations in Eq. (42) to determine the displacement field at any point in the beam. Note that the f-FEM also involves the numerical evaluation of the mass matrix, the stiffness matrix, and the force vector. The procedure to numerically evaluate the mass matrix and the force vector follows directly from classical FE formulations. The stiffness matrix of the fractional-order nonlocal system requires the evaluation of the different nonlocal matrices given in Eq. (50). Further, the attenuation function in the fractional-order model involves an end-point singularity due to the nature of the kernel [52]. The fractional-order nonlocal interactions as well as the end-point singularity are addressed in detail in Patnaik et al. [44], 45]. We emphasize that the numerical integration procedure presented in Patnaik et al. [44], 45] directly extends to the evaluation of the stiffness matrix of the FE governing equations derived in this study.

4.1. Static response

In this section, we analyse the static response of the Timoshenko beam which was obtained by solving the static part of the fractional-order FE algebraic equations in Eq. (51). In the following study, the dimensions of the beam were fixed to be $L_T=1$ m, $b_T=0.1$ m and $h_T=0.05$ m (= $L_T/20$). The simplified constitutive relations proposed in Lazar et al. [59] were used in this study:

$$\mathcal{U} = \frac{1}{2} C_{ijkl} \epsilon_{ij} \epsilon_{kl} + \frac{1}{2} I_*^2 C_{ijmn} \eta_{mnk} \eta_{ijk}$$
 (52)

The material was assumed to be isotropic with an elastic modulus E=30 GPa, Poisson's ratio v=0.3 and density $\rho=2700$ kg/m³. Further, we have assumed a symmetric and isotropic horizon of nonlocality for points sufficiently inside the domain of the beam, that is $l_{A_x}=l_{B_x}=l_f$. For points located close to a boundary, the length scales are truncated as shown in Fig. 2. Using the above material properties, we analyzed the effect of the following fractional model parameters: nonlocal strain order (α_1) , strain-gradient order (α_2) , nonlocal horizon length (l_f) and microstructure length (l_f) , on the static response of the Timoshenko beam. We merely note that the Young's modulus E and the Poisson's ratio v chosen above correspond to a general class of soft metals (e.g. lead). Given the linearity of the problem and the fact that results will be presented in a normalized form, the choice of specific elastic constants is quite immaterial for the interpretation of the results.

Although the numerical results presented below for Timoshenko beams (and later, for Mindlin plates in Section 5) are obtained for isotropic materials with simplified constitutive relations [59], the formulation is general and can account for additional material constants via the material elasticity tensors C and C (see Eq. (21)). A detailed discussion on the appropriate number of material constants necessary to capture accurately the response of complex multiscale materials can be found in Capecchi et al. [54], which outlines the Voight's and Poincaré's approach to multiscale modeling. It follows that the simplified constitutive relations does not limit the possibility of this study to use more general continuum constitutive relations. Hence, while the use of additional material constants would definitely extend the capability of the model in dealing with more complex materials, the fundamental approach and formulation remain unchanged.

We analyzed the static response of the beam subject to a uniformly distributed transverse load (UDTL) of magnitude $F_z = 10^7$ N/m for two different kinds of boundary conditions: (1) clamped-clamped (CC), and (2) simply supported at both ends (SS). For each boundary condition, we obtained the response of the beam for the following different cases:

- Case 1: the fractional-orders α_1 and α_2 were varied within the range [0.7,1] for fixed values of the nonlocal horizon length $l_f=0.5$ m (= $L_T/2$). For this case, the microstructural length was chosen as $l_*=0.005$ m ($L_T/200$) for the CC beam and $l_*=0.002$ m ($L_T/500$) for the SS beam.
- Case 2: the horizon length l_f was varied within the range [0.1, 0.5]m (= $[L_T/10, L_T/2]$) and the microstructure length l_* was varied in [0.002, 0.01]m (= $[L_T/500, L_T/100]$), for fixed values of the fractional-orders $\alpha_1 = \alpha_2 = 0.8$. Both orders were chosen in the fractional range so to obtain more general conditions (see Fig. 7).

We emphasize that, while the choice of the different fractional-model parameters were somewhat arbitrary, their specific value does not affect the generality of the results. The range of the fractional-orders α_1 and α_2 was selected following the restriction in Eq. (20). The specific ranges for l_f and l^* were chosen in order to demonstrate the ability of the fractional-order framework in capturing both stiffening and softening effects.

The numerical results, expressed in terms of the static transverse displacement and corresponding to Case 1 for the CC beam and the SS beam, are presented in Figs. 5(a) and 6(a), respectively. Similarly, the results for Case 2 subject to either CC or SS boundary conditions are provided in Figs. 5(b) and 6(b), respectively. The results presented

for each case correspond to the maximum transverse displacement observed in the beam at the mid point $(w_0(L_T/2))$. To clearly visualize the extent of softening and stiffening occurring in the beam, the maximum transverse displacement was non-dimensionalized against the maximum transverse displacement obtained for a classical Timoshenko beam in the absence of both nonlocal and strain-gradient effects. More specifically, the non-dimensional transverse displacement (\overline{w}) for each specific boundary configuration, was obtained by dividing the maximum transverse displacement of the fractional-order beam by the maximum transverse displacement of the classical beam for the same boundary condition. The maximum transverse displacement obtained for the classical CC beam was $w_0 = 8.95 \times 10^{-2}$ m and for the classical SS beam was $w_0 = 41.93 \times 10^{-2}$ m. Note that a higher value of the static displacement with respect to the classical solution indicates softening of the structure, while a lower value of the transverse displacement indicates a stiffening of the structure.

As evident from Figs. 5 and 6, the fractional-order continuum formulation is able to capture both stiffening and softening response of the Timoshenko beam depending on the choice of the nonlocal parameters. Note that the horizontal reference plane in black color denotes the non-dimensional classical solution ($\overline{w}=1$). When the transverse displacement is above this plane ($\overline{w}>1$) it indicates a softened response while, values below the plane ($\overline{w}>1$) indicate a stiffened response. The results presented for the different cases lead to the following conclusions on the specific effects of the different fractional model parameters:

- Effect of α_1 : As discussed in Patnaik et al. [45], a decrease in the value of α_1 leads to an increase in the strength of the power-law kernel that captures nonlocal interactions across the horizon of nonlocality. Consequently, the resulting formulation exhibits a greater degree of softening with respect to the classical response. Recall that for $\alpha_1 = 1$ and $l_* = 0$ (no microstructural effects), the classical local continuum formulation is recovered from the fractional-order formulation.
- Effect of l_f : recall that l_f indicates the size of the nonlocal horizon, thus by increasing the value of l_f the size of the horizon of nonlocality increases. It follows that a larger number of points within the solid is accounted contribute to the nonlocal interactions, thus the degree of nonlocality increases and so does the degree of softening of the structure
- Effect of α_2 : Recall from Section 2.1 that the strain-gradient order α_2 captures the nonlocal effects of the strain-gradients. Thus, analogous to α_1 , a decrease in the value of α_2 leads to an increase in the strength of the power-law kernel that captures nonlocal strain-gradient contributions across the horizon of nonlocality. Consequently, the resulting formulation would exhibit a softening with respect to the classical first-order strain gradient response. Note that for $\alpha_1 = 1$ and $\alpha_2 = 1$, the classical first-order strain-gradient theory is recovered from the fractional-order formulation.
- Effect of l_* : As evident from the discussion of the lattice structure in Section 2.1, the microstructural length parameter l_* plays the same role as in classical strain-gradient formulations. Thus, an increase in the value of l_* leads to a stiffer response of the structure.

The effects discussed above are schematically summarized in Fig. 7, which provides a visual representation of the resulting formulation as a function of the different parameters.

4.2. Free vibration response

In the interest of a comprehensive analysis, we analyse the effect of the different fractional model parameters on the natural frequency of transverse vibration of the Timoshenko beam. The material properties chosen for this study are the same as those provided for the static study in Section 4.1. The natural frequencies are obtained by solving the eigenvalue problem:

$$[M_T]^{-1}[K_T]\{\mathbb{U}\} = \omega_0^2\{\mathbb{U}\} \tag{53}$$

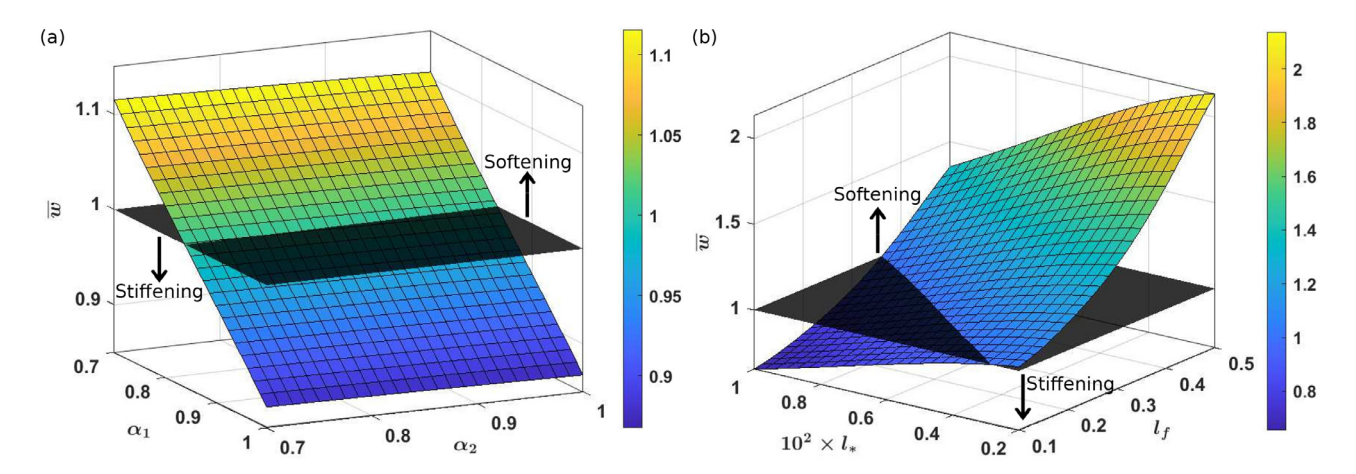


Fig. 5. Non-dimensional transverse displacement at the center point of the Timoshenko beam subject to clamped-clamped boundary conditions. Results are obtained via the fractional-order formulation. The response is parameterized for different values of (a) the fractional orders and (b) the length scales.

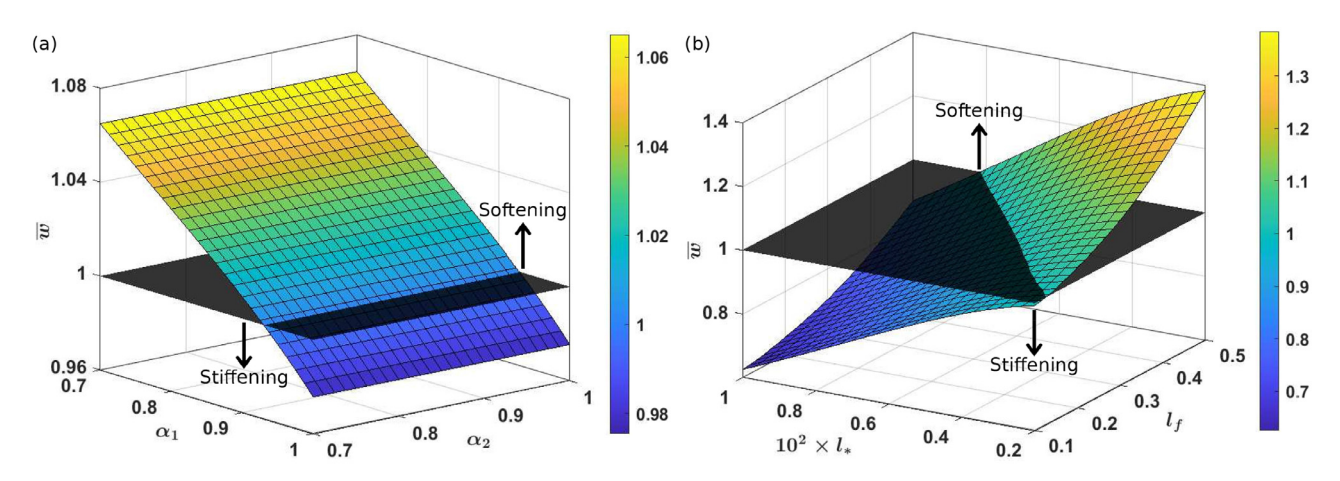


Fig. 6. Non-dimensional transverse displacement at the center point of the Timoshenko beam subject to simply supported boundary conditions. Results are obtained via the fractional-order formulation and parameterized for different values of (a) the fractional orders and (b) the length scales.

which is derived by assuming a periodic solution $\{U\} = \{U\}e^{-i\omega_0 t}$ to the homogeneous part of the algebraic FE Eq. (51). In the above assumed solution, ω_0 denotes the natural frequency of vibration, and $\mathbb U$ is the amplitude of the harmonic oscillation. Similar to Section 4.1, we obtained the natural frequencies of CC and SS beams for the two different cases: Case 1 and Case 2. The results are presented in Figs. 8 and 9. Similar to the static analysis, the natural frequency obtained for each case $(\overline{\omega}_0)$ was non-dimensionalized against the natural frequency of a classical local beam, which was found to be 53 Hz for the CC beam and 24 Hz for the SS beam. Note that a lower value of the natural frequency $(\overline{\omega}_0 < 1)$ with respect to the classical solution indicates softening of the structure, while a higher value of the natural frequency ($\overline{\omega}_0 < 1$) indicates a stiffening of the structure. Clearly, the results presented in Figs. 8 and 9 complement the discussion presented in Section 4.1, on the effect of the different fractional-order parameters on the static response of the beam.

5. Application to Mindlin plates

We extend the studies carried out in Sections 3 and 4 to develop a fractional-order analogue of the classical Mindlin plate formulation that captures both stiffening and softening response. A schematic of the undeformed rectangular plate along with the chosen Cartesian reference frame is given in Fig. 10. The top surface of the plate is identified as $z = h_M/2$, while the bottom surface is identified as $z = -h_M/2$. The domain corresponding to the mid-plane of the plate (i.e., z = 0) is de-

noted as Ω_M , such that $\Omega_M = [0, L_M] \otimes [0, B_M]$ where L_M and B_M are the length and width of the plate, respectively. The domain of the plate is identified by the tensor product $\Omega_M \otimes [-h_M/2, h_M/2]$. The edges forming the boundary of the mid-plane of the plate are denoted as $\{\Gamma_{M_X}, \Gamma_{M_y}\}$. The subscript M indicates that all the above dimensions correspond to the Mindlin plate.

For the Mindlin plate, following the coordinate system illustrated in Fig. 10, the in-plane and transverse components of the displacement field, denoted by u(x, y, z, t), v(x, y, z, t) and w(x, y, z, t) at any spatial location x(x, y, z), are related to the mid-plane displacements of the plate in the following manner:

$$u(x, y, z, t) = u_0(x, y, t) - z\theta_x(x, y, t)$$
 (54a)

$$v(x, y, z, t) = v_0(x, y, t) - z\theta_y(x, y, t)$$
 (54b)

$$w(x, y, z, t) = w_0(x, y, t)$$
 (54c)

where u_0 , v_0 , and w_0 are the mid-plane displacements of the plate along the \hat{x} , \hat{y} , and \hat{z} directions. θ_x and θ_y are the rotations of the transverse normal about the \hat{y} and \hat{x} axes, respectively. In the interest of a more compact notation, the functional dependence of the displacement fields on the spatial and the temporal variables will be implied unless explicitly expressed to be constant. Based on the above displacement fields, the non-zero strain components in the fractional-order Mindlin plate are evaluated using Eq. (22) as:

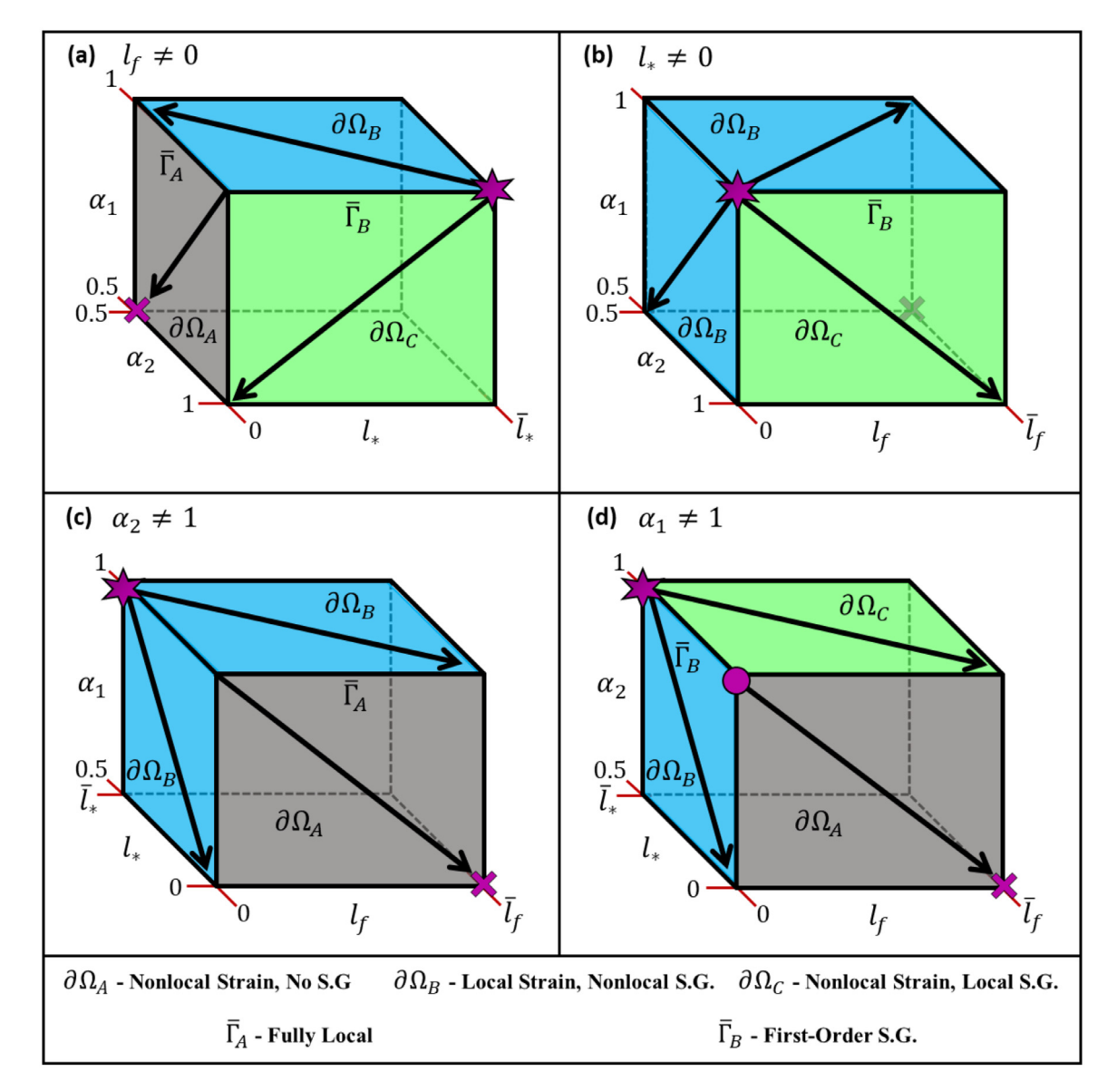


Fig. 7. Schematic illustrating the effects of the different fractional-model parameters on the direction of softening or stiffening. In the above figure, S.G. denotes strain gradient, and \bar{l}_f and \bar{l}_* indicate the upper bound on the nonlocal horizon length and the microstructural length. The direction of the solid arrow lying on a particular plane, indicates the direction of softening. It is immediate that the opposite direction would lead to stiffening. In each sub-figure, the combination of parameters that would result in the stiffest and the softest solution is indicated by a six-edged star symbol (*) and a cross symbol (×), respectively. In (d) the fully local solution is obtained at the corner indicated by a filled circular symbol.

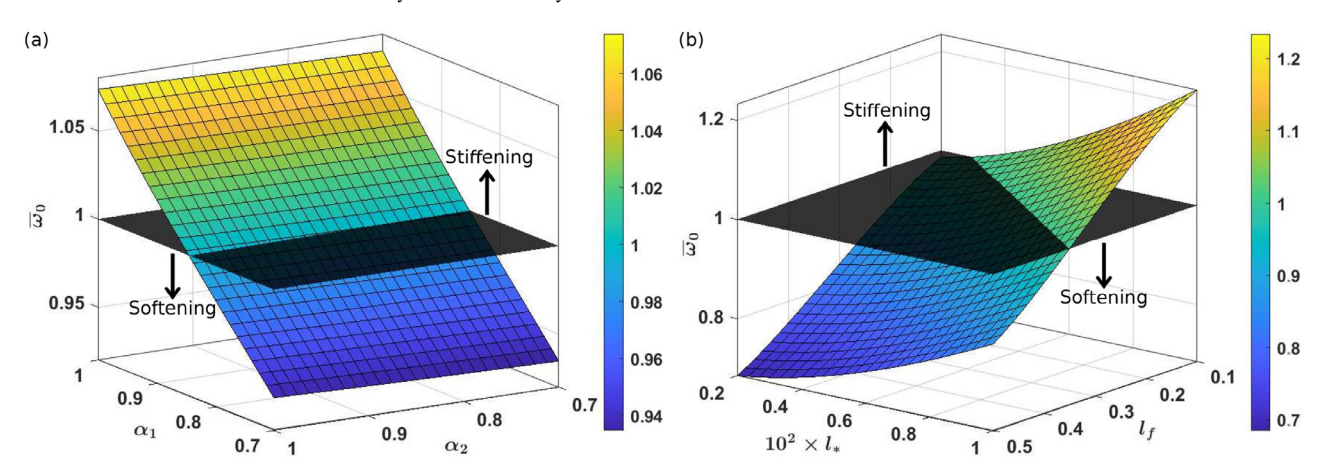


Fig. 8. Non-dimensional natural frequency of the Timoshenko beam clamped at its boundaries and parameterized for different values of (a) the fractional orders and (b) the length scales.

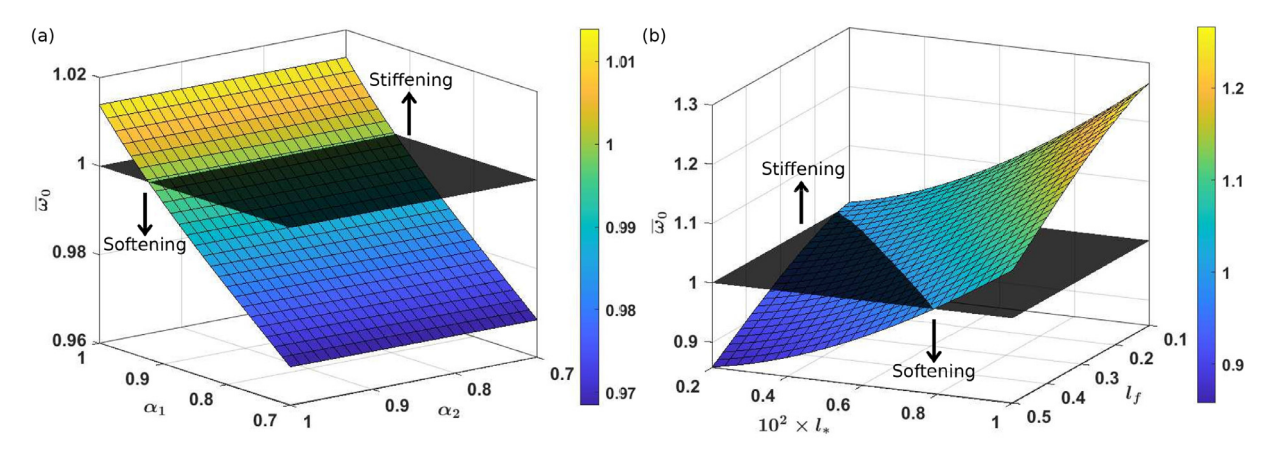


Fig. 9. Non-dimensional natural frequency of the Timoshenko beam simply-supported at its boundaries and parameterized for different values of (a) the fractional orders and (b) the length scales.

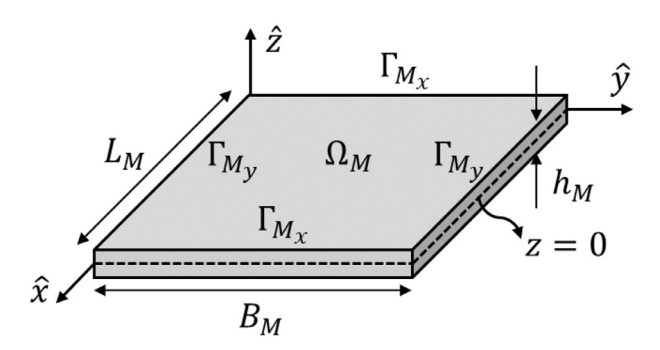


Fig. 10. Schematic of the rectangular plate illustrating the different geometric parameters.

$$\epsilon_{xx} = D_x^{\alpha_1} u_0 - z D_x^{\alpha_1} \theta_x \tag{55a}$$

$$\epsilon_{vv} = D_v^{\alpha_1} v_0 - z D_v^{\alpha_1} \theta_v \tag{55b}$$

$$\epsilon_{xy} = \frac{1}{2} \left[D_y^{\alpha_1} u_0 + D_x^{\alpha_1} v_0 - z (D_y^{\alpha_1} \theta_x + D_x^{\alpha_1} \theta_y) \right]$$
 (55c)

$$\epsilon_{xz} = \frac{1}{2} \left[D_x^{\alpha_1} w_0 - \theta_x \right] \tag{55d}$$

(a)
$$\begin{array}{c} 8 \\ 6 \\ 2 \\ 0 \\ 0.6 \\ \alpha_1 \end{array}$$
Softening
$$\begin{array}{c} 0.8 \\ 0.8 \\ 0.8 \end{array}$$

$$\epsilon_{yz} = \frac{1}{2} \left[D_y^{\alpha_1} w_0 - \theta_y \right] \tag{55e}$$

The strain-gradients developed in the plate are obtained using Eq. (24) as:

$$\eta_{xxr} = D_r^{\alpha_2} \left[D_x^{\alpha_1} u_0 - z D_x^{\alpha_1} \theta_x \right] \tag{56a} \label{eq:final_state}$$

$$\eta_{yyr} = D_r^{\alpha_2} \left[D_y^{\alpha_1} v_0 - z D_y^{\alpha_1} \theta_y \right] \tag{56b}$$

$$\eta_{xyr} = D_r^{\alpha_2} \left[\frac{1}{2} \left[D_y^{\alpha_1} u_0 + D_x^{\alpha_1} v_0 - z (D_y^{\alpha_1} \theta_x + D_x^{\alpha_1} \theta_y) \right] \right]$$
 (56c)

$$\eta_{xzr} = D_r^{\alpha_2} \left[\frac{1}{2} \left[D_x^{\alpha_1} w_0 - \theta_x \right] \right] \tag{56d}$$

$$\eta_{yzr} = D_r^{\alpha_2} \left[\frac{1}{2} \left[D_y^{\alpha_1} w_0 - \theta_y \right] \right]$$
 (56e)

where $r \in \{x, y, z\}$. While simplifying the expressions in the above equation, the following strain-gradients are obtained exactly:

$$\eta_{xxz} = D_z^{\alpha_2} [D_x^{\alpha_1} u_0] - D_z^{\alpha_2} [z D_x^{\alpha_1} \theta_x] = -D_x^{\alpha_1} \theta_x$$
 (57a)

$$\eta_{vvz} = D_z^{\alpha_2} [D_v^{\alpha_1} v_0] - D_z^{\alpha_2} [z D_v^{\alpha_1} \theta_v] = -D_v^{\alpha_1} \theta_v$$
 (57b)

$$\eta_{xyz} = \frac{1}{2} \left[D_z^{\alpha_2} [D_y^{\alpha_1} u_0 + D_x^{\alpha_1} v_0] - D_z^{\alpha_2} [z D_y^{\alpha_1} \theta_x + z D_x^{\alpha_1} \theta_y] \right]$$

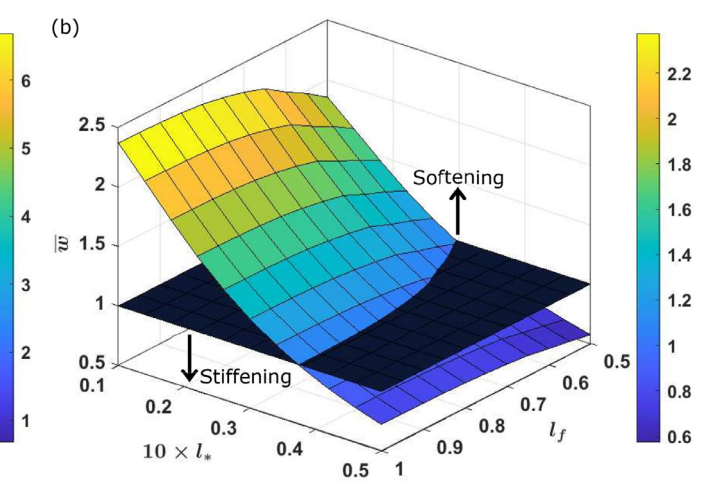


Fig. 11. Non-dimensional transverse displacement at the center point of the Mindlin plate clamped at all its edges for different values of (a) the fractional orders and (b) the length scales.

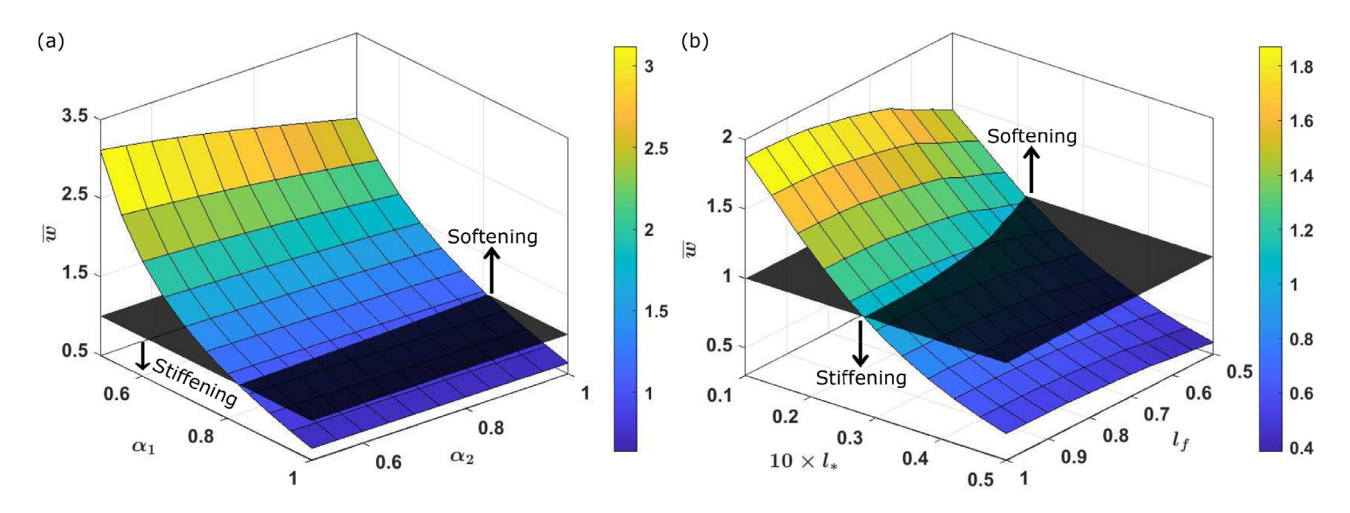


Fig. 12. Non-dimensional transverse displacement at the center point of the Mindlin plate simply-supported at all its edges parameterized for different values of (a) the fractional orders and (b) the length scales.

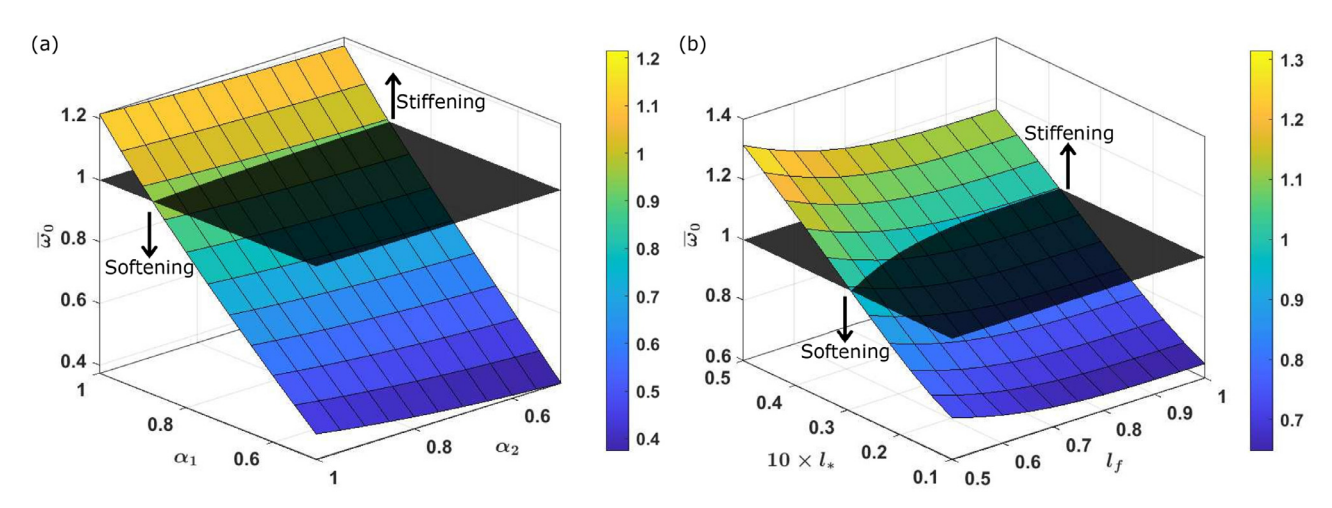


Fig. 13. Non-dimensionalized natural frequency of the Mindlin plate clamped at its edges parameterized for different values of (a) the fractional orders and (b) the length scales.

$$= -\frac{1}{2} [D_y^{\alpha_1} \theta_x + D_x^{\alpha_1} \theta_y] \tag{57c}$$

$$\eta_{xzx} = \frac{1}{2} \left[D_x^{\alpha_2} [D_x^{\alpha_1} w_0] - D_x^{\alpha_2} \theta_x \right] = -\frac{1}{2} D_x^{\alpha_2} \theta_x \tag{57d}$$

$$\eta_{xzy} = \frac{1}{2} \left[D_y^{\alpha_2} [D_x^{\alpha_1} w_0] - D_y^{\alpha_2} \theta_x \right] = -\frac{1}{2} D_y^{\alpha_2} \theta_x \tag{57e}$$

$$\eta_{xzz} = \frac{1}{2} \left[D_z^{\alpha_2} [D_x^{\alpha_1} w_0] - D_z^{\alpha_2} \theta_x \right] = 0$$
 (57f)

$$\eta_{yzx} = \frac{1}{2} \left[D_x^{\alpha_2} [D_y^{\alpha_1} w_0] - D_x^{\alpha_2} \theta_y \right] = -\frac{1}{2} D_x^{\alpha_2} \theta_y$$
 (57g)

$$\eta_{yzy} = \frac{1}{2} \left[D_y^{\alpha_2} [D_y^{\alpha_1} w_0] - D_y^{\alpha_2} \theta_y \right] = -\frac{1}{2} D_y^{\alpha_2} \theta_y \tag{57h}$$

$$\eta_{yzz} = \frac{1}{2} \left[D_z^{\alpha_2} [D_y^{\alpha_1} w_0] - D_z^{\alpha_2} \theta_y \right] = 0$$
 (57i)

Assuming small displacement gradients $(O(\varepsilon))$, the strain-gradient terms except for those provided in Eq. (57) are $O(\varepsilon^2)$. Thus, analogously to the arguments used in the development of the Timoshenko beam, for the normal strains the transverse strain-gradients are significant when compared to the in-plane gradients. When obtaining the solution via the weak form, the contribution of the in-plane strain-gradients of the normal strains can be ignored compared to the contribution of the nonzero strain-gradients in Eq. (57). This observation can also be noted

from results presented in Jafari et al. [60], where it is shown that ignoring the transverse strain-gradients of the normal strains leads to a significant change in the response of the structure, while the inclusion of the in-plane strain-gradients of the normal strains does not lead to a significant change in the response.

Using strains and strain-gradients in Eqs. (55)–(57), the first variations of the potential energy, the kinetic energy and the work done by externally applied forces are obtained as:

$$\begin{split} \delta\mathcal{U} &= \int_{\Omega_{M}} [N_{xx}\delta D_{x}^{a_{1}}u_{0} + N_{yy}\delta D_{y}^{a_{1}}v_{0} + N_{xy}\delta \left(D_{y}^{a_{1}}u_{0} + D_{x}^{a_{1}}v_{0}\right) + M_{xx}\delta D_{x}^{a_{1}}\theta_{x} \\ &+ M_{yy}\delta D_{y}^{a_{1}}\theta_{y} + M_{xy}\delta \left(\underline{D}_{y}^{a_{1}}\theta_{x} + D_{x}^{a_{1}}\theta_{y}\right) + Q_{xz}\delta (D_{x}^{a_{1}}w_{0} - \theta_{x}) \\ &+ \underline{Q}_{yz}\delta (D_{y}^{a_{1}}w_{0} - \theta_{y}) + \overline{N}_{xxz}\delta D_{x}^{a_{1}}\theta_{x} + \overline{N}_{yyz}\delta D_{y}^{a_{1}}\theta_{y} \\ &+ \overline{N}_{xyz}\delta \left(D_{y}^{a_{1}}\theta_{x} + D_{x}^{a_{1}}\theta_{y}\right) + \overline{N}_{xzx}\delta D_{x}^{a_{2}}\theta_{x} + \overline{N}_{xzy}\delta D_{y}^{a_{2}}\theta_{x} \\ &+ \overline{N}_{yzx}\delta D_{x}^{a_{2}}\theta_{y} + \overline{N}_{yzy}\delta D_{y}^{a_{2}}\theta_{y}] \mathrm{d}\Omega_{M} \end{split} \tag{58a}$$

$$\delta V = \int_{\Omega_M} \left[F_x \delta u_0 + F_y \delta v_0 + F_z \delta w_0 + M_{\theta_x} \delta \theta_x + M_{\theta_y} \delta \theta_y \right] d\Omega_M \tag{58b}$$

$$\delta T = \int_{\Omega_M} \left\{ \int_{-\frac{h}{2}}^{\frac{h}{2}} \rho \left[\left(\dot{u}_0 - z \dot{\theta}_x \right) \left(\delta \dot{u}_0 - z \delta \dot{\theta}_x \right) + \left(\dot{v}_0 - z \dot{\theta}_y \right) \left(\delta \dot{v}_0 - z \delta \dot{\theta}_y \right) \right. \\ \left. + i \dot{v}_0 \delta \dot{w}_0 \right] dz \right\} d\Omega_M$$
 (58c)

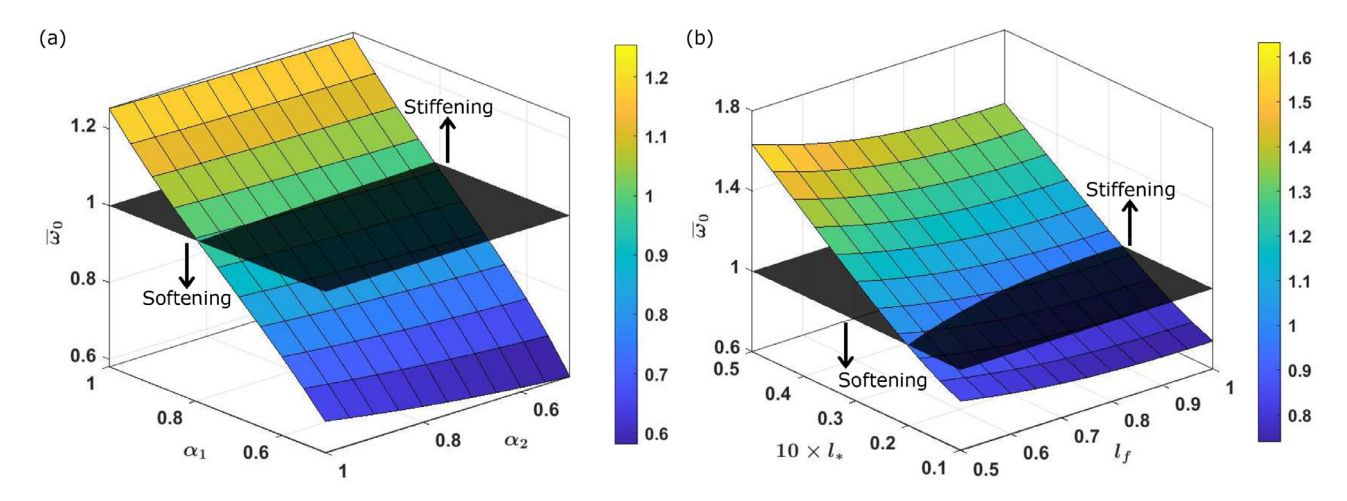


Fig. 14. Non-dimensionalized natural frequency of the Mindlin plate simply supported at its boundaries parameterized for different values of (a) the fractional orders and (b) the length scales.

Note that $\mathrm{d}\Omega_M = \mathrm{d}x\mathrm{d}y$ for a rectangular plate. $\{F_x, F_y, F_z\}$ are the external loads applied in the \hat{x} , \hat{y} , and \hat{z} directions, respectively. $\{M_{\theta_x}, M_{\theta_y}\}$ are the external moments applied about the \hat{y} and \hat{x} axes, respectively. The different stress, moment, and higher-order stress resultants in Eq. (58c) extend directly from Eq. (47).

The f-FEM for the Mindlin plates extends directly from the f-FEM formulation briefly reviewed in Section 4. We also highlight that the f-FEM for fractional-order Mindlin plates can also be found in Patnaik et al. [44]. Thus, for the sake of brevity, we do not provide all the details but we highlight the additional contributions following from the nonlocal strain-gradient terms. The expression for the stiffness matrix corresponding to the f-FEM for the Mindlin plate is:

$$[K_M] = \int_{\Omega_M} [\tilde{B}_M(\mathbf{x})]^T [S_M] [\tilde{B}_M(\mathbf{x})] d\Omega_M$$
(59)

where $[S_M]$ is the constitutive matrix of the plate and the matrix $[\tilde{B}_M(x)]$ is given as:

The details of the fractional-order derivative matrices $[\tilde{B}_{\square,r}^{n_n}(x)]$ can be found in SI and [44].

5.1. Static response

In this section, we analyze the static response of the Mindlin plate obtained via the fractional-order continuum formulation. For this purpose, the in-plane dimensions of the plate were fixed to be $L_M=1$ m and $B_M=1$ m and the thickness of the plate was taken to be $h_M=0.1$ m (= $L_M/10$). The simplified constitutive relations given in Eq. (52) were used in this study. The material was assumed isotropic with an elastic modulus E=30 GPa, Poisson's ratio v=0.3 and density $\rho=2700$ kg/m³. Further, we have assumed a symmetric and isotropic horizon of non-locality for points sufficiently inside the domain of the plate, that is

 $l_{A_{\square}}=l_{B_{\square}}=l_f, \square\in\{x,y\}.$ For points located close to a boundary, the length scales were truncated as shown in Fig. 2.

We analyzed the static response of the plate subject to a UDTL of magnitude $F_z=10^7$ Pa for two different kinds of boundary conditions: the plate clamped at all the edges (CCCC) and the plate simply supported at all ts edges (SSSS) for different combinations of the fractional model parameters. For each boundary condition, we obtained the response of the plate for the following different cases:

- Case 1: the fractional-orders α_1 and α_2 were varied within the range [0.5,1] for fixed values of the nonlocal horizon length $l_f=0.5$ m (= $L_M/2$). For this case, the microstructural length was chosen as $l_*=0.02$ m (= $L_M/50$).
- Case 2: the nonlocal horizon l_f was varied in [0.5,1]m (= $[L_M/2,L_M]$) and the microstructure length l_* was varied in [0.01,0.05]m (= $[L_M/100,L_M/20]$), for fixed values of the fractional-orders $\alpha_1=\alpha_2=0.8$.

The numerical results, in terms of the maximum transverse displacement (obtained at the mid-point of the plate), are presented in Figs. 11 and 12 for the CCCC plate and the SSSS plate, respectively. Further, similar to the Timoshenko beam, the transverse displacement obtained for each case (\overline{w}) is non-dimensionalized against the maximum transverse displacement obtained for a classical Mindlin plate without nonlocality or strain-gradient effects. The maximum transverse displacement obtained for the classical CCCC plate was $w_0 = 0.55 \times 10^{-2}$ m and for the classical SSSS plate was $w_0 = 1.55 \times 10^{-2}$ m. As evident from the Figs. 11 and 12, the fractional-order continuum formulation is able to model both stiffening and softening response of the Mindlin plate with respect to the classical formulation. The conclusions noted for the Timoshenko beam directly extend to the Mindlin plate. More specifically, the plate exhibits a stiffened response with increasing values of a_1 , a_2 and a_3 and a_4 and softened response with an increasing value of a_4 (see Fig. 7).

5.2. Free vibration response

In the following, we present the results capturing the effect of the different fractional model parameters on the natural frequency of transverse vibrations of the Mindlin plates. The material properties, loading conditions, boundary conditions and the range of the different fractional model parameters are the same as chosen for the static analysis of the Mindlin plate in Section 5.1. The results for the CCCC plate and the SSSS plate are presented in Figs. 11–14, respectively, in terms of the non-dimensionalized natural frequency $\overline{\omega}_0$. Similar to the analysis in Section 4.2, the non-dimensionalized natural frequency is obtained by

dividing the natural frequency of the fractional-order plate with the natural frequency of the classical Mindlin plate for the specific boundary condition. The natural frequency obtained for the classical CCCC plate was $\omega_0=522$ Hz and for the classical SSSS plate was $\omega_0=306$ Hz. As evident from the Figs. 11–14, the conclusions presented in Section 4.1 on the specific effects of the different fractional model parameters, hold true for the free vibration response of the Mindlin plates.

6. Conclusions

The present study leveraged the fractional-order mechanics framework to develop a unified approach to nonlocal elasticity that combines the characteristics of both integral and gradient based classical formulations. More specifically, the differ-integral nature of fractional order operators was exploited to formulate a nonlocal continuum theory capable of modeling both stiffening and softening responses in structures exhibiting size-dependent effects. The fractional-order formulation was derived by the continualization of the Lagrangian of a 1D lattice subject to long-range cohesive interactions. Then, the governing equations corresponding to a 3D continuum were derived using variational principles. The resulting nonlocal theory is frame-invariant and causal. Contrary to classical integral formulations, the fractional-order formulation of a nonlocal continuum leads to positive definite systems with well-posed governing equations. Particularly remarkable is the ability of the fractional-order continuum model to capture anomalous attenuation and dispersion without having to incorporate inertia gradients in the governing equations; otherwise needed in classical strain-gradient formulations. Consequently, the fractional theory is well suited to capture nonlocality, scale effects, and medium heterogeneity in structural problems. The ability of the fractional-order formulation to model both stiffening and softening response was exemplified by performing both static and free vibration analysis of Timoshenko beams and Mindlin plates. In conclusion, the formulation and the results presented in the study illustrated several unique features of fractional calculus and suggested that this mathematical tool could play a critical role in the development of unified and comprehensive simulation tools for modeling the response of complex nonlocal structures.

Declaration of Competing Interest

The authors declare that they do not have any financial or nonfinancial conflict of interests

CRediT authorship contribution statement

Sansit Patnaik: Methodology, Software, Formal analysis, Writing - original draft, Visualization. Sai Sidhardh: Methodology, Software, Formal analysis, Writing - original draft, Visualization. Fabio Semperlotti: Conceptualization, Methodology, Formal analysis, Writing - original draft, Writing - review & editing, Visualization, Supervision, Project administration, Funding acquisition.

Acknowledgments

The authors gratefully acknowledge the financial support of the Defense Advanced Research Project Agency (DARPA) under grant #D19AP00052, and of the National Science Foundation (NSF) under grants MOMS #1761423 and DCSD #1825837. The content and information presented in this manuscript do not necessarily reflect the position or the policy of the government. The material is approved for public release; distribution is unlimited.

Supplementary material

Supplementary material associated with this article can be found, in the online version, at 10.1016/j.ijmecsci.2020.105992

References

- Pradhan S, Murmu T. Small scale effect on the buckling of single-layered graphene sheets under biaxial compression via nonlocal continuum mechanics. Comput Mater Sci 2009:47(1):268–74.
- [2] Wang C, Murmu T, Adhikari S. Mechanisms of nonlocal effect on the vibration of nanoplates. Appl Phys Lett 2011;98(15):153101.
- [3] Reddy J, El-Borgi S, Romanoff J. Non-linear analysis of functionally graded microbeams using Eringen's non-local differential model. Int J Non Linear Mech 2014;67:308–18.
- [4] Bazant ZP. Instability, ductility, and size effect in strain-softening concrete. ASCE J Eng Mech Div 1976;102(2):331–44.
- [5] Bažant ZP. Size effect. Int J Solids Struct 2000;37(1-2):69-80.
- [6] Hollkamp JP, Sen M, Semperlotti F. Analysis of dispersion and propagation properties in a periodic rod using a space-fractional wave equation. J Sound Vib 2019;441:204–20
- [7] Patnaik S, Semperlotti F. A generalized fractional-order elastodynamic theory for nonlocal attenuating media. Proc R Soc A 2020;476(2238):20200200.
- [8] Buonocore S, Semperlotti F. Tomographic imaging of non-local media based on space-fractional diffusion models. J Appl Phys 2018;123(21):214902.
- [9] Nair S. Nonlocal Acoustic Black Hole Metastructures: Achieving Ultralow Frequency and Broadband Vibration Attenuation. Purdue University Graduate School; 2019.
- [10] Buonocore S, Sen M, Semperlotti F. Occurrence of anomalous diffusion and non-local response in highly-scattering acoustic periodic media. New J Phys 2019;21(3):033011.
- [11] Mindlin RD, Eshel N. On first strain-gradient theories in linear elasticity. Int J Solids Struct 1968;4(1):109–24.
- [12] Eringen AC. Linear theory of nonlocal elasticity and dispersion of plane waves. Int J Eng Sci 1972;10(5):425–35.
- [13] Kunin I. On foundations of the theory of elastic media with microstructure. Int J Eng Sci 1984;22(8–10):969–78.
- [14] Maugin GA. Material inhomogeneities in elasticity, 3. CRC Press; 1993.
- [15] Eringen AC. Theory of micropolar elasticity. In: Microcontinuum field theories. Springer; 1999. p. 101–248.
- [16] Trovalusci P. Molecular approaches for multifield continua: origins and current developments. In: Multiscale Modeling of Complex Materials. Springer; 2014. p. 211–78.
- [17] Peerlings RHJ, Geers MGD, De Borst R, Brekelmans WAM. A critical comparison of nonlocal and gradient-enhanced softening continua. Int J Solids Struct 2001;38(44–45):7723–46.
- [18] Aifantis EC. Update on a class of gradient theories. Mech Mater 2003;35(3-6):259-80.
- [19] Askes H, Aifantis EC. Gradient elasticity in statics and dynamics: an overview of formulations, length scale identification procedures, finite element implementations and new results. Int J Solids Struct 2011;48(13):1962–90.
- [20] Polizzotto C. Nonlocal elasticity and related variational principles. Int J Solids Struct 2001;38(42–43):7359–80.
- [21] Romano G, Barretta R. Stress-driven versus strain-driven nonlocal integral model for elastic nano-beams. Compos Part B 2017;114:184–8.
- [22] Georgiadis H, Vardoulakis I, Lykotrafitis G. Torsional surface waves in a gradient-elastic half-space. Wave Motion 2000;31(4):333–48.
- [23] Metrikine AV, Askes H. One-dimensional dynamically consistent gradient elasticity models derived from a discrete microstructure: part 1: generic formulation. Eur J Mech A/Solids 2002;21(4):555–72.
- [24] Challamel N, Zhang Z, Wang C, Reddy J, Wang Q, Michelitsch T, et al. On nonconservativeness of Eringen's nonlocal elasticity in beam mechanics: correction from a discrete-based approach. Arch Appl Mech 2014;84(9–11):1275–92.
- [25] Romano G, Barretta R, Diaco M, de Sciarra FM. Constitutive boundary conditions and paradoxes in nonlocal elastic nanobeams. Int J Mech Sci 2017;121:151–6.
- [26] Eroglu U. Perturbation approach to Eringen's local/non-local constitutive equation with applications to 1-D structures. Meccanica 2020;55:1–16.
- [27] Karim TB, McKenna GB. Comparison of surface mechanical properties among linear and star polystyrenes: surface softening and stiffening at different temperatures. Polymer 2013;54(21):5928–35.
- [28] Guha S, Sangal S, Basu S. A review of higher order strain gradient theories of plasticity: origins, thermodynamics and connections with dislocation mechanics. Sadhana 2015;40(4):1205–40.
- [29] Fuschi P, Pisano A, Polizzotto C. Size effects of small-scale beams in bending addressed with a strain-difference based nonlocal elasticity theory. Int J Mech Sci 2019;151:661–71.
- [30] Kloda L, Lenci S, Warminski J. Hardening vs softening dichotomy of a hinged-simply supported beam with one end axial linear spring: experimental and numerical studies. Int J Mech Sci 2020:105588.
- [31] Lim C, Zhang G, Reddy J. A higher-order nonlocal elasticity and strain gradient theory and its applications in wave propagation. J Mech Phys Solids 2015;78:298–313.
- [32] Li L, Hu Y. Nonlinear bending and free vibration analyses of nonlocal strain gradient beams made of functionally graded material. Int J Eng Sci 2016;107:77–97.
- [33] Li X, Li L, Hu Y, Ding Z, Deng W. Bending, buckling and vibration of axially functionally graded beams based on nonlocal strain gradient theory. Compos Struct 2017:165:250–65.
- [34] Barretta R, de Sciarra FM. Variational nonlocal gradient elasticity for nano-beams. Int J Eng Sci 2019;143:73–91.
- [35] Romano G, Barretta R, Diaco M. Iterative methods for nonlocal elasticity problems Contin Mech Thermodyn 2019;31(3):669–89.
- [36] Barretta R, de Sciarra FM. Constitutive boundary conditions for nonlocal strain gradient elastic nano-beams. Int J Eng Sci 2018;130:187–98.

- [37] Atanackovic TM, Stankovic B. Generalized wave equation in nonlocal elasticity. Acta Mech 2009;208(1–2):1–10.
- [38] Di Paola M, Failla G, Pirrotta A, Sofi A, Zingales M. The mechanically based non-local elasticity: an overview of main results and future challenges. Philos Trans R Soc A 2013;371(1993):20120433
- [39] Carpinteri A, Cornetti P, Sapora A. Nonlocal elasticity: an approach based on fractional calculus. Meccanica 2014;49(11):2551–69.
- [40] Sumelka W. Fractional calculus for continuum mechanics—anisotropic non-locality. Bull Polish Acad Sci Tech Sci 2016;64(2):361–72.
- [41] Sumelka W. On geometrical interpretation of the fractional strain concept. J Theor Appl Mech 2016;54:671–4.
- [42] Alotta G, Failla G, Zingales M. Finite-element formulation of a nonlocal hereditary fractional-order Timoshenko beam. J Eng Mech 2017;143(5):D4015001.
- [43] Sidhardh S, Patnaik S, Semperlotti F. Geometrically nonlinear response of a fractional-order nonlocal model of elasticity. Int J Non Linear Mech 2020;125:103529.
- [44] Patnaik S, Sidhardh S, Semperlotti F. Geometrically nonlinear analysis of nonlocal plates using fractional calculus. Int J Mech Sci 2020;179:105710.
- [45] Patnaik S, Sidhardh S, Semperlotti F. A Ritz-based finite element method for a fractional-order boundary value problem of nonlocal elasticity. Int J Solids Struct 2020;202:398–417.
- [46] Sidhardh S., Patnaik S., Semperlotti F.. Thermoelastic response of fractional-order nonlocal and geometrically nonlinear beams. arXiv preprint arXiv:2003102152020b;
- [47] Szabo TL. Time domain wave equations for lossy media obeying a frequency power law. J Acoust Soc Am 1994;96(1):491–500.
- [48] Fellah ZEA, Berger S, Lauriks W, Depollier C. Verification of Kramers-Kronig relationship in porous materials having a rigid frame. J Sound Vib 2004;270(4–5):865–85.
- [49] Ben-Avraham D, Havlin S. Diffusion and reactions in fractals and disordered systems. Cambridge University Press; 2000.

- [50] Polyzos D, Fotiadis D. Derivation of Mindlin's first and second strain gradient elastic theory via simple lattice and continuum models. Int J Solids Struct 2012;49(3-4):470-80.
- [51] Ortigueira MD. Fractional central differences and derivatives. IFAC Proc Vol 2006;39(11):58–63.
- [52] Kilbas AA, Srivastava HM, Trujillo JJ. Theory and applications of fractional differential equations. 204. Elsevier: 2006.
- [53] Ansari R, Oskouie MF, Rouhi H. Studying linear and nonlinear vibrations of fractional viscoelastic Timoshenko micro-/nano-beams using the strain gradient theory. Nonlinear Dyn 2017;87(1):695–711.
- [54] Capecchi D, Ruta G, Trovalusci P. Voigt and Poincaré's mechanistic-energetic approaches to linear elasticity and suggestions for multiscale modelling. Arch Appl Mech 2011;81(11):1573–84.
- [55] Tuna M, Kirca M, Trovalusci P. Deformation of atomic models and their equivalent continuum counterparts using Eringen's two-phase local/nonlocal model. Mech Res Commun 2019;97:26–32.
- [56] Sidhardh S, Ray M. Dispersion curves for rayleigh–lamb waves in a micro-plate considering strain gradient elasticity. Wave Motion 2019;86:91–109.
- [57] Tarasov VE. Fractional vector calculus and fractional Maxwell's equations. Ann Phys 2008;323(11):2756–78.
- [58] Yurkov A. Elastic boundary conditions in the presence of the flexoelectric effect. JETP Lett 2011;94(6):455–8.
- [59] Lazar M, Maugin GA, Aifantis EC. Dislocations in second strain gradient elasticity. Int J Solids Struct 2006;43(6):1787–817.
- [60] Jafari A, Shah-enayati SS, Atai AA. Size dependency in vibration analysis of nano plates; one problem, different answers. Eur J Mech A/Solids 2016;59:124–39.